71-27,602

CHANG, Lu-Chung, 1923-
TURBULENT BOUNDARY-LAYER GROWTH FAR
DOWNSTREAM IN A SLOWLY EXPANDING HYPERSONIC
NOZZLE.

The University of Oklahoma, D.Engr., 1971
Engineering, aeronautical

University Microfilms, A XEROX Company, Ann Arbor, Michigan

THE UNIVERSITY OF OKLAHOMA

GRADUATE COLLEGE

TURBULENT BOUNDARY-LAYER GROWTH FAR DOWNSTREAM IN A SLOWLY EXPANDING HYPERSONIC NOZZLE

A DISSERTATION

SUBMITTED TO THE GRADUATE FACULTY

in partial fulfillment of the requirement for the

degree of

DOCTOR OF ENGINEERING

BY

LU-CHUNG CHANG

Norman, Oklahoma

1971

TURBULENT BOUNDARY-LAYER GROWTH FAR DOWNSTREAM

IN A SLOWLY EXPANDING HYPERSONIC NOZZLE

APPROVED BY

M. L. Rasmussen

C. W. Bert

E. F. Blick

J. E. Francis

DISSERTATION COMMITTEE

ACKNOWLEDGEMENT

The writer takes the opportunity to express his deep appreciation to the Aerospace, Mechanical, and Nuclear Engineering School for its continuous support for this study. His appreciation also goes to Dr. Rasmussen whose mathematical ingenuity helped a lot in the analysis of the problem. He also wishes to thank Dr. Bert, Dr. Blick and Dr. Francis for their invaluable suggestions in preparing this paper.

TABLE OF CONTENTS

TABLES

ILLUSTRATIONS

LIST OF SYMBOLS

A	geometric nozzle cross-sectional area ratio, $(R/r_*)^2$
A_e	effective nozzle area ratio, $\rho_* u_* / \rho_1 u_1$
a	initial nozzle expansion angle for power-law family of nozzle shapes
C	constant
C_{fw}	friction coefficient at wall
C_f	friction coefficient
$D(U_1)$	integral function associated with boundary layer displacement thickness
E	constant
$E(U_1)$	integral function associated with boundary layer energy thickness
g	enthalpy profile parameter
h	enthalpy
J	total enthalpy
K	a constant associated with mass flow ratio of inviscid nozzle flow
M	Mach number
$N(U)$	a defined function of κU_1
Pr	Prandtl number
Q	dimensionless mass flow ratio

q	heat transfer rate
R	Reynolds number or nozzle section radius
R_{eff}	a defined flow parameter
R_e	characteristic Reynolds number
r	distance from nozzle axis
S	a constant in Sutherland's viscosity law
S_T	Stanton number
s	power-law nozzle expansion parameter
U	dimensionless velocity
u	axial velocity of the flow
v	radial velocity of the flow
W	a defined function of flow conditions
x	longitudinal axis of the nozzle
Y	transformed coordinate
y	coordinate from wall parpendicular to x
Z	flow parameter in terms of Mach number
β	turbulent empirical constant
γ	specific heat ratio
Δ	thermal boundary-layer thickness
δ	boundary-layer thickness
δ^*	displacement thickness
$\delta^{(t)}$	linear displacement thickness
ϵ	eddy viscosity

η	a defined Reynolds number
θ	boundary-layer momentum thickness
κ	turbulent empirical constant
μ	molecular viscosity
ρ	density
ξ	non-dimensionalized longitudinal axis
	frictional stress
ϕ	boundary-layer energy thickness

Subscripts:

$(\ )_0$	Stagnation state unless specified
$(\ )_1$	core flow condition
$(\ )_a$	associated with Model A
$(\ )_b$	associated with Model B
$(\ )_t$	initial condition imposed at throat of the nozzle
$(\ )_w$	wall condition
$(\ )_*$	throat condition

SUMMARY

An analysis of turbulent boundary-layer growth far downstream in a slowly expanding hypersonic nozzle is presented. Transverse curvature, boundary-layer displacement, and heat transfer are taken into account. A compressible form of a universal law-of-the-wall velocity profile allows so-called relaminarization to be predicted for certain nozzle shapes. Numerical results for various flow conditions and different nozzle shapes are illustrated. Comparison is made with a limited amount of experimental data. Because of the large temperature differences between the wall and free stream, it appears that a more precise viscosity law than a linear variation with temperature is needed to gain good agreement with experiment.

I. INTRODUCTION

The behavior of the boundary-layer growth far downstream in a hypersonic nozzle is a very complicated matter. In addition to the fact the boundary layer becomes very thick, such that displacement and transverse curvature effects become important, it has been observed that a turbulent boundary layer tends to undergo transition toward a laminar-like form. This so-called relaminarization was observed experimentally in a supersonic nozzle by Sergienko and Gretsov (1959). This conclusion was reached indirectly by Rasmussen and Karamcheti (1966) who found that their general analysis based on power-law profiles agreed with experiment only when the power-law profile was selected between the conventional type of turbulent behavior and that of a laminar boundary layer. Their analysis could not predict that reverse transition would occur, but merely infer that it did by comparison with observed displacement-thickness data.

The purpose of this investigation is to devise an analytical method for computing the boundary-layer growth in a hypersonic nozzle that allows the transition from turbulent to laminar-like flow to be predicted. There are a number of difficulties associated with the development of such a method. First, the development of conventional turbulent boundary layer is not altogether well understood, especially when compressible flow is involved. Moreover, reverse transition in incompressible flows has been studied only recently. In addition, thick boundary layers in hypersonic nozzle flows require consideration of viscous interaction and transverse curvature effects. This greatly complicated the analysis. Finally, the high temperature usually associated with hypersonic nozzle flows require the consideration of real-gas effects. In this study, we shall concentrate on the reverse transition of a compressible turbulent boundary layer in a hypersonic nozzle. Towards these ends, a number of simplifying approximations will be made. The scheme of analysis will be akin to that of Steczkowski (1969), but will be generalized to include heat transfer and transverse curvature.

Several experimental studies have been conducted concerning the so-called relaminarization of a turbulent boundary layer in the presence of a favorable pressure gradient that is sufficiently large. A detailed description of the phenomena involved has been given by Kline (1967). According to Kline, the earliest verified cases of relaminarization are due to Sternberg (1954) and Senoo (1957) in this country and Sergienko and Gretsov (1959) of the Soviet Union. All of these investigators studied accelerated flows and comfirmed that relaminarization occurred. None of them obtained detailed measurements of the process, nor did any of them correlate the phenomenon. Kline found that there are ways to achieve relaminarization other than accelerating the flow. Patel and Head (1968) presented a comprehensive discussion of the topic for incompressible flow of which various characteristics of relaminarization were described quantitatively in terms of the magnitude of the necessary favorable pressure gradient.

The incorporation of the phenomena observed for incompressible flow into a model for compressible flow appropriate for hypersonic nozzles presents a certain amount of difficulty. The corresponding reversion in a hypersonic nozzle has not been experimentally examined, especially with regard to the structure of the reversion. Whereas the reversion in incompressible flow has been observed to occur fairly abruptly, observations of abrupt changes in the boundary-layer characteristics of hypersonic nozzle flow have not been reported. In this investigation, a model is developed that allows for gradual transition from turbulent to laminar flow. A number of the gross features of relaminarization can thus be accounted for. The results of the analysis will be compared with a limited amount of data obtained by Kemp and Sreekanth (1969) for hypersonic flow.

There are several alternative lines of analysis that incorporate compressibility into turbulent boundary-layer calculations. One method, initiated by Wilson (1950) and Van Driest (1951), makes use of the motion of a mixing length and allows for a variable density. Maise and McDonald (1968) discussed mixing length and viscosity as applied to compressible boundary layers and give a list of pertinent references. Recently, Bucknell and Beckwith (1970) extended these ideas to include non-equilibrium effects. Another line of analysis makes use of a compressibility transformation that transforms the compressible form of the boundary-layer equations to a incompressible form. This approach was proposed by Mager (1958), Coles (1964) and Lewis, Kubota, and Webb (1970), to name a few. A list of pertinent references can be found in a paper by Laufer (1968) who discussed some of the problems associated with compressibility transformation. This study combines the compressibility and transverse curvature in a single transformation. Further correlation of the transformed variable with an assumed shear-stress distribution leads to a generalized form of the law-of-the-wall for compressible flow. The resulting formula allows for simple mathematical analysis, yields satisfactory agreement with known limiting situations, and, most importantly, allows for a smooth transition from turbulent to laminar-like behavior.

In this study, a perfect gas will be assumed in order to simplify the analysis. In hypersonic tunnels that utilize helium, for instance, this is not a severe limitation. The experimental data of Kemp and Sreekanth (1969), used for comparison with the analysis, are obtained with helium as the test gas. Heat transfer is handled by means of an integral form of the energy equation and an assumed enthalpy profile across the boundary layer. Approximate analytical solution and numerical solutions to the momentum and energy equations are compared with displacement-thickness and velocity-profile data.

II. FORMULATION OF THE PROBLEM

1. The Boundary-Layer Equations for Axisymmetric Flow

In the formulation of turbulent flow, the flow variables are represented by the sum of a mean and a fluctuation component. Accordingly, the viscous stress and heat transfer are each expressed in two parts. With this understanding in applying Williams' (1963) slender-nozzle approximation, one obtains the boundary-layer equations in cylindrical coordinates (Sketch 1.) as the following:

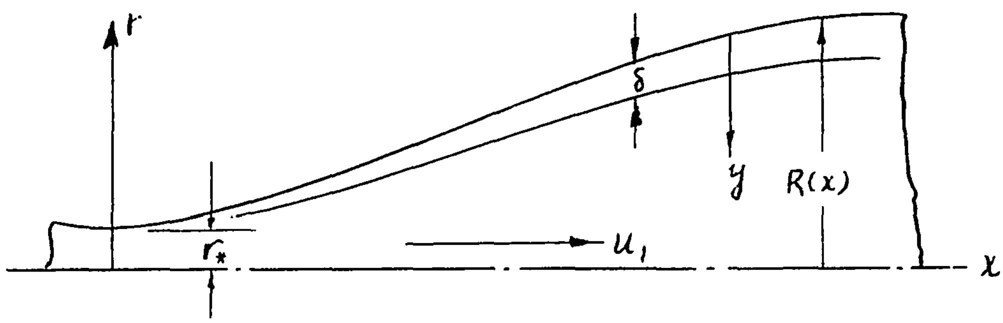

Sketch 1.

Mass: $$\frac{\partial \rho u r}{\partial x} + \frac{\partial \rho v r}{\partial r} = 0 \tag{1.1}$$

Momentum: $$\frac{\partial \rho u^2 r}{\partial x} + \frac{\partial \rho u v r}{\partial r} = -r\frac{dp}{dx} - \frac{\partial r \tau}{\partial r} \tag{1.2}$$

Energy: $$\frac{\partial \rho u J r}{\partial x} + \frac{\partial \rho v J r}{\partial r} = \frac{\partial}{\partial r}(r u \tau - r q) \tag{1.3}$$

where

$$J = h + u^2/2 \tag{1.4}$$

$$\tau = \mu \frac{\partial u}{\partial r} + \tau' \tag{1.5}$$

$$q = -k \frac{\partial T}{\partial r} + q' \tag{1.6}$$

The primed quantities are contributions from turbulent fluctuations. Equations(1.1-1.3) are valid for both laminar and turbulent flows. If the turbulent effects are specified, the method of solution would essentially be the same. As the boundary-layer growth is the main concern of this study, the Von Karman momentum-integral method is the appropriate one to be employed. Instead of the flow variables in the above equations, we deal with the so-called boundary-layer displacement thicknesses--mass, momentum, and energy. For the chosen coordinate system (Sketch 1.), they are defined as:

$$\delta^* = \frac{1}{R}\int_{R-\delta}^{R} \left(1 - \frac{\rho u}{\rho_1 u_1}\right) r\,dr \tag{1.7}$$

$$\theta = \frac{1}{R}\int_{R-\delta}^{R} \left(\frac{\rho u}{\rho_1 u_1}\right)\left(1 - \frac{u}{u_1}\right) r\,dr \tag{1.8}$$

$$\phi = \frac{1}{R}\int_{R-\delta}^{R} \frac{\rho u}{\rho_1 u_1}\left(1 - \frac{J - h_w}{h - h_w}\right) r\,dr \tag{1.9}$$

II. FORMULATION OF THE PROBLEM

1. The Boundary-Layer Equations for Axisymmetric Flow

In the formulation of turbulent flow, the flow variables are represented by the sum of a mean and a fluctuation component. Accordingly, the viscous stress and heat transfer are each expressed in two parts. With this understanding in applying Williams' (1963) slender-nozzle approximation, one obtains the boundary-layer equations in cylindrical coordinates (Sketch 1.) as the following:

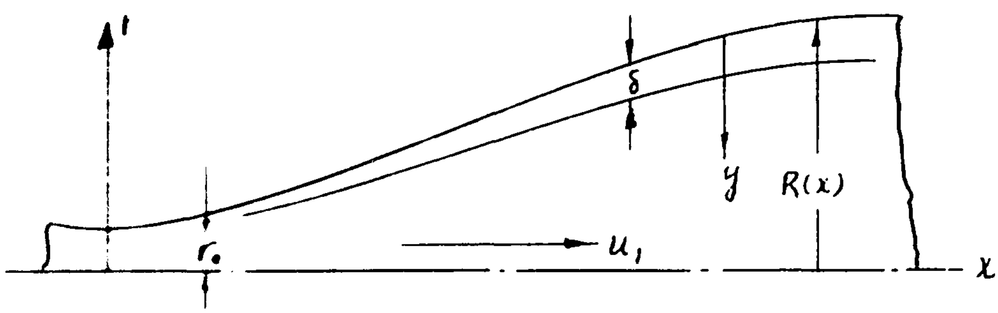

Sketch 1.

Mass:
$$\frac{\partial \rho u r}{\partial x} + \frac{\partial \rho v r}{\partial r} = 0 \tag{1.1}$$

Momentum:
$$\frac{\partial \rho u^2 r}{\partial x} + \frac{\partial \rho u v r}{\partial r} = -r \frac{dp}{dx} - \frac{\partial r \tau}{\partial r} \tag{1.2}$$

Energy: $$\frac{\partial \rho u J r}{\partial x} + \frac{\partial \rho v J r}{\partial r} = \frac{\partial}{\partial r}(r u \tau - r q) \qquad (1.3)$$

where

$$J \equiv h + u^2/2 \qquad (1.4)$$

$$\tau \equiv \mu \frac{\partial u}{\partial r} + \tau' \qquad (1.5)$$

$$q \equiv -k \frac{\partial T}{\partial r} + q' \qquad (1.6)$$

The primed quantities are contributions from turbulent fluctuations. Equations(1.1-1.3) are valid for both laminar and turbulent flows. If the [illegible] effects are specified, the method of soluti[illegible]y be the same. As the boundary-layer [illegible]cern of this study, the Von Karman mo[illegible] the appropriate one to be employe[illegible]riables in the above equations, w[illegible]d boundary-layer displacement thickne[illegible], and energy. For the chosen coordinate sy[illegible]n 1.), they are defined as:

$$\delta^* = \frac{1}{R}\int_{R-\delta}^{R}\left(1 - \frac{\rho u}{\rho_1 u_1}\right) r\,dr \qquad (1.7)$$

$$\theta = \frac{1}{R}\int_{R-\delta}^{R}\left(\frac{\rho u}{\rho_1 u_1}\right)\left(1 - \frac{u}{u_1}\right) r\,dr \qquad (1.8)$$

$$\phi = \frac{1}{R}\int_{R-\delta}^{R}\frac{\rho u}{\rho_1 u_1}\left(1 - \frac{J - h_w}{h - h_w}\right) r\,dr \qquad (1.9)$$

where δ is the boundary-layer thickness.

It is seen from these expressions that δ^*, θ, and ϕ all have the dimension of length whereas δ^*/R, θ/R, and ϕ/R are dimensionless areas. In terms of $y = R-r$, these expressions can be rewritten as:

$$\delta^* = \int_0^\delta \left(1 - \frac{\rho u}{\rho_1 u_1}\right)\left(1 - \frac{y}{R}\right) dy \tag{1.10}$$

$$\theta = \int_0^\delta \frac{\rho u}{\rho_1 u_1}\left(1 - \frac{u}{u_1}\right)\left(1 - \frac{y}{R}\right) dy \tag{1.11}$$

$$\phi = \int_0^\delta \frac{\rho u}{\rho_1 u_1}\left(1 - \frac{I - h_w}{h - h_w}\right)\left(1 - \frac{y}{R}\right) dy \tag{1.12}$$

The factor (1-y/R) in the integrals represents the transverse curvature effect characterizing the boundary-layer flow in an axisymmetric nozzle. When $y/R \rightarrow 0$, the expressions (1.10-1.12) reduce to the usual form of two dimensional flow.

Introducing a dimensionless "effective" cross-section area, A_e, suggested by one-dimensional gasdynamics, and a dimensionless geometric cross-section area, A, defined by

$$A_e = \rho_* u_* / \rho_1 u_1 \tag{1.13}$$

$$A = (R/r_*)^2 \tag{1.14}$$

where r_* is the radius at the throat, one casts the equations

(1.1-1.3) into the form:

Mass: $$\frac{A}{A_e}\left(1-\frac{2\delta^*}{R}\right)=Q \tag{1.15}$$

Momentum: $$\frac{d\rho_1 u_1^2 R\theta}{dx}+\rho_1 u_1 R\delta^*\frac{du}{dx}=-R\tau_w \tag{1.16}$$

Energy: $$\frac{d\rho_1 u_1 R\phi}{dx}=\frac{Rq_w}{h_e-h_w} \tag{1.17}$$

In equation (1.15), Q is the ratio of total mass flow for the viscous to inviscid case. It is seen from the equation that when $\delta^*=0$ and $A_e=A$--inviscid flow--, Q equals 1. Generally δ^*/R will be very small near the throat and the flow will be nearly sonic, and Q will thus be a number near unity. Except for regions in the immediate vicinity of the throat, we can set Q=1 whenever $\delta^*/R \ll 1$ near the throat.

It is convenient to work with a friction coefficient defined as

$$C_f=-\tau_w/\left(\tfrac{1}{2}\rho_1 u_1^2\right) \tag{1.18}$$

It is also convenient to define a friction coefficient that is normalized with the wall density instead of the free-stream density, that is,

$$C_{fw}=-\tau_w/\left(\tfrac{1}{2}\rho_w u_1^2\right)=C_f\,\rho_1/\rho_w \tag{1.19}$$

The appropriate dimensionless heat-transfer coefficient is given by the Stanton number:

$$S_T = q_w / \left[\rho_1 u_1 (h_o - h_w) \right] \tag{1.20}$$

The equations (1.16) and (1.17) can be written in different forms. In terms of θ and ϕ , they become

$$\frac{d\theta}{dx} + \theta \left[\frac{d \ln (\rho_1 u_1 R)}{dx} + \left(1 + \frac{\delta^*}{\theta}\right) \frac{d \ln u_1}{dx} \right] = \frac{C_{fw}}{2} \frac{\rho_w}{\rho_1} \tag{1.21}$$

$$\frac{d\phi}{dx} + \phi \frac{d \ln (\rho_1 u_1 R)}{dx} = S_T \tag{1.22}$$

The Reynolds number based on δ^*, θ , and ϕ are defined as:

$$R_{\delta^*} \equiv \frac{\rho_1 u_1 \delta^*}{\mu_w} \tag{1.23}$$

$$R_\theta \equiv \frac{\rho_1 u_1 \theta}{\mu_w} \tag{1.24}$$

$$R_\phi \equiv \frac{\rho_1 u_1 \phi}{\mu_w} \tag{1.25}$$

If the temperature of the nozzle wall remains constant or approximately so, one derives from equations (1.16-1.17) that

$$\frac{dR_\theta}{dx} + R_\theta \left[\frac{d \ln R}{dx} + \left(1 + \frac{\delta^*}{\theta}\right) \frac{d \ln u_1}{dx} \right] = \frac{1}{2} C_{fw} \rho_w u_1 / \mu_w \tag{1.26}$$

$$\frac{dR_\phi}{dx} + R_\phi \frac{d \ln R}{dx} = S_T \rho_1 u_1 / \mu_w \tag{1.27}$$

Equations (1.21) and (1.22) can be combined to read:

$$\frac{d}{dx}\left(\frac{\phi}{\theta}\right) - \frac{\phi}{\theta}\left(1+\frac{\delta^*}{\theta}\right)\frac{d\,\ln u_1}{dx} = \frac{\phi}{\theta}\left(\frac{\delta_T}{\phi} - \frac{C_{fw}}{2\theta}\frac{\rho_w}{\rho_1}\right) \tag{1.28}$$

Equations (1.15), (1.26), and (1.28) constitute the basic equations used in this analysis.

To make further progress, we must make approximations for the velocity and enthalpy profiles across the boundary-layer. This is taken up in the next section.

2. Eddy Viscosity and the Compressible Law-of-the-Wall

The momentum-integral method allows the selection of a velocity profile that satisfies certain boundary conditions of the flow field. This study specifies the stress and the eddy viscosity distributions so that the volocity profile is contained in these forms.

The turbulent form of stress is defined as:

$$\tau = \mu\left(1+\frac{\epsilon}{\mu}\right)\frac{\partial u}{\partial y} \tag{2.1}$$

where μ is the molecular viscosity and ϵ is the eddy viscosity. Two models of stress distribution are considered:

(A) $$\tau = \tau_w(1-y/R) \tag{2.2}$$

(B) $$\tau = \tau_w(1-y/R)(1-Y/\Delta) \tag{2.3}$$

The factor (1-y/R) is a transverse curvature term that is inserted to accommadate a transformation to be introduced shortly. If this factor is ignored, expression (2.2) assumes that the stress is constant across the boundary layer, which, of course, is a common approximation for incompressible turbulent boundary layers (see Schlichting (1964), for example). Expression (2.3) improves on Model A by allowing τ to vanish at the outer edge of the boundary layer, $Y=\Delta$, where Y and Δ are transformed variables.

In equation (1.10-1.12), there are factors of transverse curvature and density in addition to velocity. In order to transform these integrals into an "incompressible form", one introduces

$$Y = \int_0^y \frac{\rho}{\rho_w}\left(1 - \frac{y}{R}\right) dy \tag{2.4}$$

$$\Delta = \int_0^\delta \frac{\rho}{\rho_w}\left(1 - \frac{y}{R}\right) dy \tag{2.5}$$

The variable Y then takes care of the effects of both transverse curvature and density variation. The stress at the wall can be written in terms of Y:

(A) $$\tau_w = \frac{\rho\mu}{\rho_w}\left(1 + \frac{\epsilon}{\mu}\right) \frac{\partial u}{\partial Y} \tag{2.6}$$

(B) $$\tau_w\left(1 - \frac{Y}{\Delta}\right) = \frac{\rho\mu}{\rho_w}\left(1 + \frac{\epsilon}{\mu}\right) \frac{\partial u}{\partial Y} \tag{2.7}$$

It is now convenient to introduce the so-called friction velocity

$$u_\tau = \left(\frac{\tau_w}{\rho_w}\right)^{1/2} \tag{2.8}$$

so that non-dimensional velocity and transformed normal coordinate can be defined as

$$U = u/u_\tau \tag{2.9}$$

$$\eta = \rho_w u_\tau Y/\mu_w \tag{2.10}$$

$$\eta_\Delta = \frac{\rho_w u_\tau \Delta}{\mu_w} \tag{2.10a}$$

We further assume that viscosity varies linearly with temperature and can be approximated by the following law:

$$\frac{\mu}{\mu_w} = C \; \frac{T}{T_w} \tag{2.11}$$

where

$$C = \left[\sqrt{\frac{T}{T_w}} \quad \frac{T_w + S}{T + S} \right]_{\text{average}}$$

is some suitably averaged constant. The constant C arises from the Sutherland viscosity law. Treating C as a constant allows a linear variation with temperature and a corresponding simplification in the analysis to follow. The parameter S appearing in the expression for C is a characteristic temperature for a particular gas (for air, S=110° K). With this approximation, we now can write

$$\frac{\rho \mu}{\rho_w \mu_w} = C = \text{constant} \tag{2.12}$$

In terms of the new variables and the approximation (2.12), equations (2.6) and (2.7) take the form

(A) $$1 = C\left(1 + \frac{\epsilon}{\mu}\right) \frac{\partial U}{\partial \eta} \tag{2.13}$$

(B) $$1 - \frac{\eta}{\eta_\Delta} = C\left(1 + \frac{\epsilon}{\mu}\right) \frac{\partial U}{\partial \eta} \tag{2.14}$$

We now follow Rasmussen and Karamcheti (1965) and Spalding (1961) and assume that the ratio ϵ/μ is some function of U. In particular we shall use the simpler form utilized by Rasmussen and Karamcheti:

$$\frac{\epsilon}{\mu} = \frac{2K}{\beta}(\sinh KU - KU) \tag{2.15}$$

Here K =0.4 and β =10 were found to reproduce conventional values appearing in the logarithmic law-of-the-wall. Substitution of (2.15) into (2.13) and (2.14) and integration yields

(A) $$\eta = C\left\{U + \frac{2}{\beta}\left[\cosh KU - \frac{(KU)^2}{2} - 1\right]\right\} \tag{2.16}$$

(B) $$\eta\left(1 - \frac{\eta}{2\eta_\Delta}\right) = C\left\{U + \frac{2}{\beta}\left[\cosh KU - \frac{(KU)^2}{2} - 1\right]\right\} \tag{2.17}$$

Recalling that $\eta = \eta_\Delta$ when $u=u_1$, we can rearrange these expressions to read

(A) $$\frac{Y}{\Delta} = \frac{N(U)}{N(U_1)} \tag{2.18}$$

(B) $$\frac{Y}{\Delta} = 1 - \left[1 - \frac{N(U)}{N(U_1)}\right]^{1/2} \tag{2.19}$$

where

$$N(U) = C\left\{U + \frac{2}{\beta}\left[\cosh KU - \frac{(KU)^2}{2} - 1\right]\right\} \tag{2.20}$$

Since $U = U_1\frac{U}{U_1} = U_1\frac{u}{u_1}$, equations (2.18) and (2.19) give velocity profile for u/u_1 as a function of Y/Δ with $U_1 = \sqrt{2/C_{fw}}$ as a parameter. Before we discuss the relation further, it is useful to represent U_1 (or C_{fw}) as a function of Reynolds number, which is a more useful variable to use as a parameter in plotting the velocity profiles. We consider this in the next section.

3. Boundary-Layer Displacement Thicknesses

3.1 Momentum Thickness

(A) In terms of Y and U_1, the momentum thickness (1.11) can be written as:

$$\theta = \frac{\rho_w}{\rho_1}\int_0^{\Delta} \frac{u}{u_1}\left(1-\frac{u}{u_1}\right) dY = \frac{\rho_w u_\tau}{\rho_1 u_1}\int_0^{\Delta} U\left(1-\frac{U}{U_1}\right) dY \qquad (3.1)$$

The Reynolds number R_θ can then be derived from this expression in the following form:

$$R_\theta \equiv \frac{\rho_1 u_1 \theta}{\mu_w} = \int_0^{\eta_\Delta} U\left(1-\frac{U}{U_1}\right) d\eta = \int_0^{U_1} U\left(1-\frac{U}{U_1}\right)\frac{d\eta}{dU}\,dU$$

$$= C\left\{\frac{U_1^2}{6} + \frac{2}{K\beta}\left[\sinh KU_1 - \frac{2(\cosh KU-1)}{KU_1} - \frac{(KU_1)^3}{12}\right]\right\} \qquad (3.2)$$

Since $U_1 = (2/C_{fw})^{1/2}$, this gives R_θ as a function of C_{fw}.

When $U_1 >> 1$, this expression reduces to

$$\frac{R_\theta}{C} = \frac{1}{K\beta}e^{KU_1} \qquad (3.3)$$

or $$U_1 = \frac{1}{K}\left[\ln(R_\theta/C) + \ln K\beta\right] \qquad (3.4)$$

which has the same form as the well known logarithmic friction law (see Schlichting (1964)) for incompressible turbulent flow. For $U_1 \to 0$, expression (3.2) yields

$$\frac{R_\theta}{C} = U_1^2/6 = 1/(3C_{fw}) \tag{3.5}$$

which corresponds to a linear velocity profile and is to be regarded as the limiting form for laminar flow. A plot of C_{fw} versus R_θ is shown in Fig. 1.

Equation (2.18) can be written as

$$\frac{Y}{\Delta} = \frac{U + \frac{2}{\beta}\left[\cosh \kappa U - \frac{(\kappa U)^2}{2} - 1\right]}{U_1 + \frac{2}{\beta}\left[\cosh \kappa U_1 - \frac{(\kappa U_1)^2}{2} - 1\right]} \tag{3.6}$$

A number of velocity profiles versus Y/Δ for different Reynolds number R_θ can be plotted by means of equations (3.6) and (3.2). This is shown in Fig. 2. For large Reynolds numbers the viscous sublayer is very thin, and most of the profile has the logarithmic form characteristic of turbulent boundary layers (except for the outer "wake" portion of the boundary layer). As the Reynolds number decreases, the viscous sublayer grows to a larger percentage of the boundary layer. As the Reynolds number tends to zero, the viscous sublayer has become nearly the entire boundary layer. For Model A, the limiting profile is linear.

(B) From equation (2.19), we deduce that

$$\frac{\partial\eta}{\partial U} = \frac{\frac{dN(U)}{dU}}{\left[1-\frac{N(U)}{N(U_1)}\right]^{1/2}} = -2C\,N(U_1)\frac{d}{dU}\left[1-\frac{N(U)}{N(U_1)}\right]^{1/2} \qquad (3.7)$$

The same procedure as for Model A in deriving R_θ leads to

$$R_\theta = \frac{\rho_1 U_1 \theta}{\mu_w} = \int_0^{U_1} U\left(1-\frac{U}{U_1}\right)\frac{d\eta}{dU}\,dU$$

$$= -2C\,N(U_1)\int_0^{U_1} U\left(1-\frac{U}{U_1}\right)\frac{d}{dU}\left[1-\frac{N(U)}{N(U_1)}\right]^{1/2} dU \qquad (3.8)$$

Integrating by parts, one obtains

$$R_\theta = 2C\,N(U_1)\int_0^{U_1}\left[1-\frac{N(U)}{N(U_1)}\right]^{1/2}\left(1-\frac{2U}{U_1}\right)dU \qquad (3.9)$$

This expression can not be evaluated analytically except for $U_1 \to 0$, in which case, we have

$$R_\theta/C = 4U_1^2/15 = 8/(15\,C_{fw}) \qquad (3.10)$$

This differs from the corresponding value of Model A by a factor of 1.60. Numerical integration also shows that R_θ versus C_{fw} on a logarithmic scale almost parallels Model A all the way over to $R_\theta/C = 10^{10}$. The plot is shown in Fig. 1.

Equation (2.19) in association with (3.8) constitutes the velocity profile versus Y/Δ for a certain R_θ. Several examples are shown in Fig. 3. The plot reveals the same aspects as for the Model A version. For Model B, however, the limiting profile as $R_\theta \to 0$ is parabolic, having the form $\frac{u}{u_1} = \frac{Y}{\Delta}\left(2 - \frac{Y}{\Delta}\right)$. This profile is probably more representative of laminar flow.

The smooth transition behavior is also displayed in the plot of C_{fw} versus R_θ for either Model A or B. As is seen in Fig.1, when C_{fw} decreases, R_θ increases. For large R_θ, C_{fw} decreases logarithmically in the conventional manner of incompressible turbulent flow. As R_θ decreases, a smooth transition takes place until C_{fw} varies inversely to R_θ in a manner reflecting laminar behavior. In both Models A and B, the Reynolds number R_θ is the parameter that reflects the nature of the boundary layer.

3.2 Energy Thickness

Along with the stress or velocity profile, it is necessary to assume a form for the enthalpy profile. Following Rasmussen and Karamcheti (1966), we assume a modification of the Crocco integral that has the form

$$\frac{J - h_w}{h_c - h_w} = g \frac{u}{u_1} + (1-g)\left(\frac{u}{u_1}\right)^2 \tag{3.11}$$

Here we introduced a parameter g that we evaluate by requiring that (3.11) satisfy the following conditions at the wall:

$$q_w = k\left(\frac{\partial T}{\partial y}\right)_w = \frac{k}{C_p}\left(\frac{\partial h}{\partial y}\right)_w \tag{3.12}$$

$$\tau_w = -\mu\left(\frac{\partial u}{\partial y}\right)_w \tag{3.13}$$

We determine that

$$g \equiv 2 S_T P_r / C_f \tag{3.14}$$

where

$$P_r \equiv C_p \mu / k \tag{3.15}$$

is the Prandtl number evaluated at the wall. Expression (3.11) can also be written as :

$$h = h_w\left[1 - \left(\frac{u}{u_1}\right)^2\right] + (h_{c_1} - h_w)\, g \frac{u}{u_1}\left(1 - \frac{u}{u_1}\right) + h_1\left(\frac{u}{u_1}\right)^2 \tag{3.16}$$

Because the pressure is constant across the boundary layer, this expression will be used to evaluate the density distribution across the boundary layer.

By means of equation (3.11) we can write the energy thickness (1.12) in the form:

$$\phi = \frac{\rho_w}{\rho_1}\int_0^{\Delta} \frac{u}{u_1}\left[1 - g\,\frac{u}{u_1} - (1-g)\left(\frac{u}{u_1}\right)^2\right] dY$$

$$= \theta + \frac{\rho_w}{\rho_1}(1-g)\int_0^{\Delta}\left(\frac{u}{u_1}\right)^2\left(1 - \frac{u}{u_1}\right) dY \qquad (3.17)$$

It follows that the Reynolds number based on energy thickness is

$$R_\phi \equiv \frac{\rho_1 u_1 \phi}{\mu_w} = R_\theta + (1-g)\,\frac{\rho_w u_1}{\mu_w}\,\frac{u_\tau}{u_1}\int_0^{\Delta} U\,\frac{U}{U_1}\left(1 - \frac{U}{U_1}\right) dY$$

$$= R_\theta + (1-g)\int_0^{U_1} U\,\frac{U}{U_1}\left(1 - \frac{U}{U_1}\right)\frac{d\eta}{dU}\,dU$$

$$= R_\theta + (1-g)\int_0^{U_1} \eta\left(\frac{2U}{U_1} - \frac{3U^2}{U_1^2}\right) dU \qquad (3.18)$$

For the two models of stress distribution, we obtain:

(A) $$R_\phi = R_\theta + (1-g)\,C\left\{\frac{U_1^2}{12} + \frac{2}{\kappa\beta}\left[\sinh \kappa U_1 - \frac{4\cosh \kappa U_1}{\kappa U_1} - \frac{2}{\kappa U_1} + \frac{6\sinh \kappa U_1}{(\kappa U_1)^2} - \frac{(\kappa U_1)^3}{20}\right]\right\} = R_\theta + (1-g)\,E_a(U_1) \qquad (3.19)$$

$$\text{(B)} \qquad R_\phi = R_\theta + (1-g)\frac{2CN(U_1)}{U_1}\int_0^{U_1}\left[1-\frac{N(U)}{N(U_1)}\right]^{\frac{1}{2}}\left(2U-\frac{3U^2}{U_1}\right)dU$$

$$= R_\theta + (1-g)E_b(U_1) \qquad (3.20)$$

where

$$E_a(U_1) = C\left\{\frac{U_1^2}{12} + \frac{2}{K\beta}\left[\sinh KU_1 - \frac{4\cosh KU_1}{KU_1} - \frac{2}{KU_1}\right.\right.$$

$$\left.\left. + \frac{6\sinh KU_1}{(KU)^2} - \frac{(KU_1)^3}{20}\right]\right\} \qquad (3.21)$$

and

$$E_b(U_1) = \frac{2CN(U_1)}{U_1}\int_0^{U_1}\left[1-\frac{N(U)}{N(U_1)}\right]\left(2U-\frac{3U^2}{U_1}\right)dU \qquad (3.22)$$

From equation (3.19) and (3.20), one notices that

$$R_\phi/R_\theta = \phi/\theta = 1+(1-g)E(U_1)/R_\theta \qquad (3.23)$$

where

$$E(U_1) = E_a(U_1) \quad \text{for Model A}$$

$$= E_b(U_1) \quad \text{for Model B}$$

The behavior of the functions $E(U_1)/R_\theta$ is shown in Fig. 4 and 5. It is seen that they vary slowly for $KU_1 \gg 1$. As $KU_1 \rightarrow \infty$,

$$E_a(U_1)/R_\theta \rightarrow 1, \quad \text{for } C=1$$

and

$$E_b(U_1)/R_\theta \rightarrow 0.9, \quad \text{for } C=1$$

For the convenience of numerical calculation, it would be a good approximation to set

$$E_a(U_1)/R_\theta = E_b(U_1)/R_\theta = 1 \quad \text{for} \quad U_1 > 10$$

This covers the maximum Reynolds number or the minimum friction coefficient attainable for the problem on hand.

The ratio R_ϕ/R_θ differs from unity for all values of κU_1 unless $g = 1$. It becomes constant only when both $E(U_1)/R_\theta$ and g are constant.

3.3 Displacement Thickness

Because the pressure is constant across the boundary layer, the density ratio for a perfect gas is the inverse of the enthalpy ratio given by (3.16), that is

$$\frac{\rho_1}{\rho} = \frac{h}{h_1} = \frac{h_w}{h_1}\left[1-\left(\frac{u}{u_1}\right)^2\right] + \frac{h_o - h_w}{h_1}\, g\, \frac{u}{u_1}\left(1-\frac{u}{u_1}\right) + \left(\frac{u}{u_1}\right)^2 \qquad (3.24)$$

With this result the displacement thickness (1.10) can be written

$$\delta^* = \left(\frac{h_o - h_w}{h_1}\, g + \frac{h_w}{h_o} - 1\right)\theta + \int_0^\Delta \left(1 - \frac{u}{u_1}\right) dY \qquad (3.25)$$

For the two stress models A and B we obtain

$$\text{(A)} \qquad \int_0^\Delta \left(1 - \frac{u}{u_1}\right) dY = \frac{\mu_w}{\rho_w u_\tau} \int_0^{U_1} \left(1 - \frac{u}{u_1}\right) \frac{d\eta}{dU}\, dU$$

$$= C\,\frac{\mu_w}{\rho_1 u_1}\,\frac{\rho_1}{\rho_w}\left\{\frac{U_1^2}{2}+\frac{2}{\kappa\beta}\left[\sinh\kappa U_1-\frac{(\kappa U_1)^3}{6}-\kappa U_1\right]\right\} \tag{3.26}$$

(B) $$\int_c^\Delta\left(1-\frac{u}{u_1}\right)dY = 2CN(U_1)\frac{\mu_w}{\rho_w u_\tau}\left\{1-\int_0^{U_1}\left[1-\frac{N(U)}{N(U_1)}\right]^{1/2}\frac{dU}{U_1}\right\}$$

$$= 2CN(U_1)\frac{\mu_w}{\rho_1 u_1}\,\frac{\rho_1}{\rho_w}\left\{U_1-\int_0^{U_1}\left[1-\frac{N(U)}{N(U_1)}\right]^{1/2}dU\right\} \tag{3.27}$$

The Reynolds number based on δ^* can be expressed as

$$R_{\delta^*}\equiv\frac{\rho_1 u_1\delta^*}{\mu_w}=\left(\frac{h_1-h_w}{h_1}\,\mathcal{g}+\frac{h_w}{h_1}-1\right)\mathcal{g}+\frac{\rho_1}{\rho_w}\,D(U_1) \tag{3.28}$$

where $D(U_1)$ is a function corresponding to $E(U_1)$ in the expression of R_ϕ, defined as

(A) $$D(U_1)=D_a(U_1)=C\left\{\frac{U_1^2}{2}+\frac{2}{\kappa\beta}\left[\sinh\kappa U_1-\frac{(\kappa U_1)^3}{6}-\kappa U_1\right]\right\} \tag{3.29}$$

(B) $$D(U_1)=D_b(U_1)=2CN(U_1)\left\{U_1-\int_0^{U_1}\left[1-\frac{N(U)}{N(U_1)}\right]^{1/2}dU\right\} \tag{3.30}$$

We also note the form by equation (3.28)

$$\frac{\delta^*}{\theta}=\frac{R_{\delta^*}}{R_\theta}=\frac{h_0-h_w}{h_1}\,\mathcal{g}+\frac{h_w}{h_1}-1+\frac{\rho_1}{\rho_w}\,\frac{D(U_1)}{R_\theta} \tag{3.31}$$

It is useful to express this relation in terms of the Mach number M_1, or more conveniently the combination

$$\frac{h_0}{h_1}\equiv Z = 1+\frac{\gamma-1}{2}M_1^2 \tag{3.32}$$

For a perfect gas we then obtain

$$\frac{h_w}{h_1} = \frac{T_w}{T_1} = \frac{\rho_1}{\rho_w} = \frac{T_w}{T_c} Z \tag{3.33}$$

Equation (3.31) can then be written as:

$$1 + \frac{\delta^*}{\theta} = \left\{ \left(1 + \frac{T_w}{T_o}\right) g + \frac{T_w}{T_o} \left[1 + \frac{D(U_1)}{R_\theta} \right] \right\} Z \tag{3.34}$$

The variation of $D(U_1)/R_\theta$ as a function of κU_1 for Models A and B is plotted in Figs. 4 and 5. They vary very slowly when $\kappa U_1 > 10$. It would be a good approximation to take $D(U_1)/R_\theta = 1$ in this range.

4. Velocity and Density Profiles

The inverse transformation to expression (2.4) is

$$\int_0^Y \frac{\rho_w}{\rho}\, dY = \int_0^y \left(1 - \frac{y}{R}\right) dy \qquad (4.1)$$

The two sides can be evaluated separately:

$$\int_0^Y \frac{\rho_w}{\rho}\, dY = \frac{\mu_w}{U_\tau} \int_0^U \frac{1}{\rho} \frac{d\eta}{du}\, du \qquad (4.2)$$

$$\int_0^y \left(1 - \frac{y}{R}\right) dy = y\left(1 - \frac{y}{2R}\right) \qquad (4.3)$$

One is led to the relation between y and U as follows:

$$\frac{y\left(1 - \frac{y}{2R}\right)}{\delta\left(1 - \frac{\delta}{2R}\right)} = \frac{\int_0^U \frac{h}{h_w} \frac{d\eta}{du}\, du}{\int_0^{U_1} \frac{h}{h_w} \frac{d\eta}{du}\, du} \qquad (4.4)$$

This is the relationship of velocity distribution across the boundary layer in terms of the physical coordinate y. Equation (4.4) can be solved for y/δ in the form

$$\frac{y}{\delta} = \frac{R}{\delta}\left\{1 - \left[1 - \frac{\delta}{R}\left(2 - \frac{\delta}{R}\right) F_n\right]^{1/2}\right\} \qquad (4.5)$$

where

$$F_n = \int_0^U \frac{h}{h_w} \frac{d\eta}{du}\, du \Bigg/ \int_0^{U_1} \frac{h}{h_w} \frac{d\eta}{du}\, du \qquad (4.6)$$

The ratio of boundary-layer thickness to nozzle radius, δ/R, is known when a certain problem has been solved. It is a measure of the transverse curvature effect.

After u/u_1 has been determined as a function of y/δ by means of expression (4.4) the density and temperature distributions can be determined from equation (3.24), which we rewrite here:

$$\frac{\rho_1}{\rho} = \frac{T}{T_1} = \left\{ \frac{T_w}{T} \left[1-\left(\frac{u}{u_1}\right)^2\right] + \left(1-\frac{T_w}{T_0}\right) g \frac{u}{u_1}\left(1-\frac{u}{u_1}\right)\right\} Z - \left(\frac{u}{u_1}\right)^2 \qquad (4.7)$$

The function, Fn, defined in expression (4.6) can be evaluated with reference to Eq.(4.7) and the two stress models:

$$\text{(A)} \quad \frac{d\eta}{du} = C\left[1+\frac{2\kappa}{\beta}(\sinh \kappa u - \kappa u)\right] \qquad (4.8)$$

$$\text{(B)} \quad \frac{d\eta}{du} = -2CN(u)\frac{d}{du}\left[1-\frac{N(u)}{N(u_1)}\right]^{1/2} \qquad (4.9)$$

where N(U) is defined in expression (2.20). The integral in (4.6) for Model A is presented in Appendix I and that for Model B must be evaluated numerically.

For both models A and B, it can be seen that the velocity profile in the physical coordinates has the following functional relation:

$$\frac{y}{\delta} = Fn\left(\frac{u}{u_1}, \frac{\delta}{R}, \frac{T_w}{T_0}, Z, g, R_\theta\right) \qquad (4.10)$$

For a given problem δ/R, g, R_θ will be functions of Z and T_w/T_0.

5. Core-Flow Approximation and Summary of Equations

In the mass-conservation equation (1.15), it was introduced two area ratios, an "effective" area ratio A_e, and a geometric area ratio A. If there were no boundary layer, these two area ratios would be equal. The effective area ratio arises from isentropic quasi-one-dimensional gasdynamics (see Liepmann & Roshko (1958), for example) and is a function of Mach number. For a thermally and calorically perfect gas, we have

$$A_e = \frac{\rho_* u_*}{\rho_1 u_1} = K Z^{\frac{\gamma+1}{2(\gamma-1)}} (Z-1)^{-1/2} \tag{5.1}$$

where

$$Z \equiv 1 + \frac{\gamma-1}{2} M_1^2 \qquad K \equiv \left(\frac{2}{\gamma+1}\right)^{\frac{\gamma+1}{2(\gamma-1)}} \left(\frac{2}{\gamma-1}\right)^{-1/2} \tag{5.2}$$

The function $A_e(Z)$ reflects the effective area ratio of the inviscid core flow.

The geometric area ratio, $A \equiv (R/r_*)^2$, is regarded as a given function of x, the distance down the nozzle measured from the throat. For this study, we shall select a family of nozzle shapes with the following form, appropriate for flows downstream of the throat:

$$A = \left(1 + \frac{a}{s} \xi\right)^{2s} \tag{5.3}$$

where $\quad \xi = x/r_*$ (5.4)

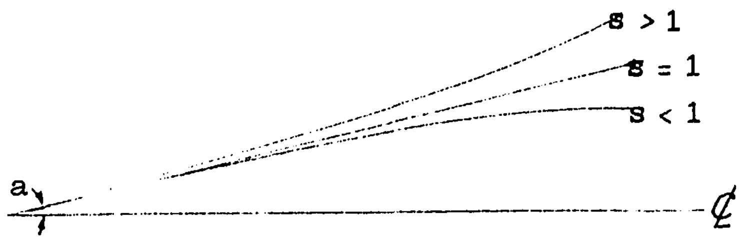

Sketch 2.

This family of shapes is described in terms of two parameters, a and s, as shown in Sketch 2. The parameter a denotes the initial expansion angle of the nozzle. The parameter s describes the rate at which the nozzle cross-sectional area grows. When s=1, the nozzle is a cone of semivertex angle a. When $s > 1$, the nozzle grows faster than a cone. When $s < 1$, the nozzle grows slower than a cone.

Because the inviscid core flow is a function of Mach number, it is convenient to use the variable Z as the independent variable in the problem instead of the non-dimensional distance. We thus write equations (1.26-1.28) in the form

$$\frac{dR_\theta}{dZ} + R_\theta\left[\frac{d\ln R}{dZ} + \left(1 + \frac{\delta^*}{\theta}\right)\frac{d\ln u_1}{dZ}\right] = \frac{C_{fw}}{2}\left(\frac{T_c}{T_w}\right)^2 \frac{Re^*}{A_e}\,\frac{1}{Z}\,\frac{d\xi}{dZ} \tag{5.5}$$

$$\frac{dR_\phi}{dZ} + R_\phi\frac{d\ln R}{dZ} = S_T\,\frac{Re^*}{A_e}\,\frac{T_c}{T_r}\,\frac{d\xi}{dZ} \tag{5.6}$$

$$\frac{d}{dZ}\left(\frac{\phi}{\theta}\right) - \frac{\phi}{\theta}\left(1 + \frac{\delta^*}{\theta}\right)\frac{d\ln u_1}{dZ} = \frac{R_{e*}}{A_e}\,\frac{C_{fw}}{2R_\theta}\,\frac{d\xi}{dZ}\left[\frac{T_0}{T_w}\,\frac{\mathcal{J}}{P_r} - \left(\frac{T_0}{T_w}\right)^2\frac{1}{Z}\,\frac{\phi}{\theta}\right] \tag{5.7}$$

Here $$R_{e*} \equiv \frac{\rho_* u_* r_*}{\mu_0} \tag{5.8}$$

is the characteristic Reynolds number for the problem. In this expression, ρ_* and u_* are some values of density and velocity, r_* is the radius of the throat, and μ_0 is the viscosity of the gas evaluated at the reservoir temperature. It is now useful to express the derivatives $\frac{dR}{dZ}$, $\frac{du_1}{dZ}$, and $\frac{d\xi}{dZ}$ that appear in equations (5.5-5.7) as functions of Z.

By means of the definition

$$Z \equiv \frac{h_0}{h_1} = 1 + \frac{\gamma-1}{2}M_1^2 = 1 + \frac{1}{2}\,\frac{u_1^2}{h_0}\,Z \tag{5.9}$$

we can deduce that

$$\frac{d\ln u_1}{dZ} = \frac{1}{2Z(Z-1)} \tag{5.10}$$

If we also notice that

$$R = r_*(A/A_e)^{1/2}\,A_e^{1/2} \tag{5.11}$$

then it follows that

$$\frac{d\ln R}{dZ} = \frac{d\ln(A/A_e)^{1/2}}{dZ} + \frac{d\ln A_e^{1/2}}{dZ} \tag{5.12}$$

Making use of equations (5.4) and (5.11), we obtain

$$\frac{d\xi}{dZ} = \frac{1}{2a}\left(\frac{A}{A_e}\right)^{1/2}A_e^{1/2}\left[\frac{d\ln(A/A_e)}{dZ} + \frac{d\ln A_e}{dZ}\right] \tag{5.13}$$

This expression can be reduced to the form obtained by Rasmussen and Karamcheti (1964) (see Appendix II). The parameter A/A_e appears in the mass conservation equation (1.15). From equation (5.1) we obtain

$$\frac{d \ln A_e}{dZ} = \frac{2Z - \gamma - 1}{2(\gamma - 1)Z(Z-1)} \tag{5.14}$$

Writing the above equations in terms of the ratio A/A_e suggests a systematic scheme of approximate solution. When the boundary layer is very thin, $\delta^*/R \ll 1$, we see from (1.15) that $A/A_e \approx 1$. Setting $A/A_e = 1$, we can simplify equations (5.12) and (5.13) to read

$$\frac{d \ln R}{dZ} = \frac{d \ln A_e^{1/2}}{dZ} = \frac{2Z - \gamma - 1}{4(\gamma-1)Z(Z-1)} \tag{5.15}$$

$$\frac{d\xi}{dZ} = K^{1/2s} \frac{2Z - \gamma - 1}{4a(\gamma-1)Z(Z-1)} Z^{\frac{\gamma+1}{4s(\gamma-1)}} (Z-1)^{-1/4s} \tag{5.16}$$

Substituting equations (5.10), (5.15), (5.16), and (3.23) into equations (5.5) and (5.7), we obtain

$$\frac{dR_\theta}{dZ} + \frac{R_\theta}{2(Z-1)} \left\{ \frac{2Z-\gamma-1}{2(\gamma-1)Z} - \left(1 - \frac{T_w}{T_0}\right) g + \frac{T_w}{T_c}\left[1 + \frac{D(U_1)}{R_\theta}\right]\right\}$$

$$= \left(\frac{T_c}{T_w}\right)^2 \frac{R_e C_{fw}(2Z-\gamma-1)}{8a(\gamma-1)} K^{\frac{1-2s}{2s}} Z^{\frac{\gamma+1-2s(5\gamma-3)}{4s(\gamma-1)}} (Z-1)^{-\frac{1+2s}{4s}} \tag{5.17}$$

$$\frac{d}{dZ}\left[(1-g)\frac{E(U_1)}{R_\theta}\right] - \left[1+(1-g)\frac{E(U_1)}{R_\theta}\right] \frac{\left(1-\frac{T_w}{T_0}\right)g + \frac{T_w}{T_0}\left[1+\frac{D(U_1)}{R_\theta}\right]}{2(Z-1)}$$

$$= \frac{R_{e*}\, C_{fw}}{2R_\theta}\left\{\frac{T_c}{T_w}\frac{g}{P_r} - \left(\frac{T_c}{T_w}\right)^2 \frac{1}{Z}\left[1+(1-g)\frac{E(U_1)}{R_\theta}\right]\right\} \frac{2Z-\gamma-1}{4a(\gamma-1)} \cdot$$

$$K^{\frac{1+2s}{2s}}\; Z^{\frac{\gamma+1-2s(3\gamma-1)}{4s(\gamma-1)}}\; (Z-1)^{-\frac{1+2s}{4s}} \qquad (5.18)$$

Since C_{fw} and U_1 are functions of R_θ, these are two equations for R_θ and g. Higher approximations will be discussed in a later chapter. The parameters that appear in equations (5.17) and (5.18) are a, s, Pr, γ, Re_*, and T_w/T_0. These are to be specified for a given problem. The functional relations between C_{fw}, U_1, $D(U_1)$, $E(U_1)$, and R_θ depend on the alternative use of model A or B by the velocity profile in the boundary layer.

Equations (5.17) and (5.18) will be solved by a numerical integration procedure. In addition, an approximate asymptotic solution will be obtained for very large Mach numbers.

6. Displacement Effect

As was pointed out in Section 1, the mass displacement δ^*/R is actually a dimensionless area, which is appropriate for thick axisymmetric boundary layers. It is useful to establish for a dimensionless displacement thickness, which is a more conventional result taken from experience with thin boundary layers. We first note that we can write the identity

$$\frac{\delta^*}{R} \equiv \frac{R_{\delta^*}}{R_\theta} \frac{R_\theta}{R_{e*}} \frac{T_w}{T_0} \left(\frac{A_e}{A} \right)^{1/2} A_e^{1/2} \tag{6.1}$$

In this expression we set $\mu_w/\mu_c = T_w/T_0$ (C=1). Also recall that

$$\frac{R_{\delta^*}}{R_\theta} = \frac{\delta^*}{\theta} = \left\{ \left(1 - \frac{T_w}{T_0}\right) g + \frac{T_w}{T_0} \left[1 + \frac{D(\omega_1)}{R_\theta} \right] \right\} Z - 1 \tag{6.2}$$

is derived from equations (3.31) and (3.32), and Re_* is the characteristic Reynolds number defined by equation (5.8). The Reynolds number R_θ is determined as a function of Z from the zeroth approximation, and A_e is also a function of Z. The factor A/A_e is unknown at this point. Since $R=r_* A^{1/2}$, however, we can define $R_{eff}=r_* A_e^{1/2}$, and equation (6.1) can be

$$\frac{\delta^*}{R_{eff}} = \frac{R_{\delta^*}}{R_\theta} \frac{R_\theta}{R_{e*}} \frac{T_w}{T_0} A_e^{1/2} \tag{6.3}$$

This ratio can be determined from the zeroth approximation since A/A_e now does not appear.

When δ^*/R_{eff} is known, we can solve for A_e/A by starting with equation (1.14) written in the following form (Q set equal to unity):

$$\frac{A}{A_e}\left[1-\frac{2\delta^*}{R_{eff}}\left(\frac{A_e}{A}\right)^{1/2}\right]=1 \tag{6.4}$$

This is a quadratic equation for (A_e/A) , which has the solution

$$\left(\frac{A_e}{A}\right)^{1/2}=\left[1+\left(\frac{\delta^*}{R_{eff}}\right)^2\right]^{1/2}-\frac{\delta^*}{R_{eff}} \tag{6.5}$$

It now follows that

$$\frac{\delta^*}{R}=\frac{\delta^*}{R_{eff}}\,\frac{R_{eff}}{R}=\frac{\delta^*}{R_{eff}}\left(\frac{A_e}{A}\right)^{1/2}=\frac{\delta^*/R_{eff}}{\delta^*/R_{eff}+\left[1+(\delta^*/R_{eff})^2\right]^{1/2}} \tag{6.6}$$

Thus δ^*/R is a function of δ^*/R_{eff}, which can be determined at various levels of approximation.

Consider now a displacement thickness, $\delta^{(t)}$, as shown in Sketch 3. The shaded region

Sketch 3.

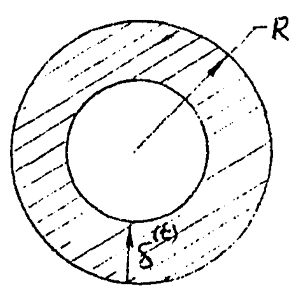

is the displacement area, $2\pi R^2(\delta^*/R)$. The relationship between the displacement area and thickness is

$$2\pi R\delta^* = \pi R^2 - \pi R^2 (1 - \frac{\delta^{(t)}}{R})^2$$

or $$\frac{\delta^{(t)}}{R} = 1 - (1 - \frac{2\delta^*}{R})^{1/2} = 1 - (\frac{A_e}{A})^{1/2} \qquad (6.7)$$

Thus, $\delta^{(t)}/R$ is also a function of δ^*/R_{eff}.

When δ^*/R_{eff} is very small, then δ^*/R and $\delta^{(t)}/R$ are approximately equal. However, for thick boundary layers δ^*/R_{eff} can vary from zero to infinity, whereas equations (6.6) and (6.7) show that $0 \leq \delta^*/R \leq \frac{1}{2}$ and $0 \leq \delta^{(t)}/R \leq 1$.

With the above expressions, it is now possible to set down a successive approximation scheme.

Recalling that in establishing equations (5.17) and (5.18), we ignored the derivative of "A_e/A" in the expressions of $\frac{d\ln R}{dz}$ and $\frac{d\xi}{dz}$ (see (5.12) and (5.13)) for lack of data on δ^* or A_e/A. The equations so established are henceforth termed as zeroth approximation in reference to the effect of boundary-layer displacement. With the solution of equations (5.17) and (5.18), one can then evaluate A_e/A by equation (6.5). Also from equation (6.5), one can derive that

$$\frac{d\ln(A_e/A)}{dZ} = \frac{-2R_{eff}}{(1+R_{eff}^2)^{1/2}}\left[\frac{\theta}{\delta^*}\frac{d}{dZ}(\frac{\delta^*}{\theta}) + \frac{1}{2}\frac{d\ln A_e}{dZ} + \frac{1}{R_\theta}\frac{dR_\theta}{dZ}\right] \qquad (6.8)$$

The terms $\frac{\theta}{\delta^*}\frac{d}{dZ}\left(\frac{\delta^*}{\theta}\right)$ and $\frac{d \ln A_e}{dZ}$ can be evaluated from equations (3.31) and (5.14) respectively; and $\frac{1}{R_\theta}\frac{dR_\theta}{dZ}$ is the solution of equations (5.17) and (5.18). The value of $d(A_e/A)/dZ$ so obtained being put into equations (5.12) and (5.13) and substituted in the numerical integration structure of equations (5.5) and (5.7), one can then obtain another solution as the first approximation--also in reference to the displacement effect. This process can be stepped up for even higher approximations. However, this study worked out the zeroth approximation only. The procedure to obtain higher approximations are laid down here for reference.

III. SOLUTION FOR LARGE MACH NUMBERS

1. Asymptotic Approximations

It is useful to consider approximations appropriate for large Mach numbers. When $Z \gg 1$, equations (5.17) and (5.18) take the following asymptotic forms:

$$\frac{dR_\theta}{dZ} + \frac{B}{Z} R_\theta = W \frac{C_{fw}}{2} Z^{b} \tag{1.1}$$

$$\frac{d}{dZ}\left[(1-g)\frac{E(u_1)}{R_\theta}\right] - \frac{1}{2Z}\left(2B - \frac{1}{\gamma-1}\right)\left[1+(1-g)\frac{E(u_1)}{R_\theta}\right] = \frac{C_{fw}}{2R_\theta}\frac{T_0}{T_w} W g Z^{b-1} \tag{1.2}$$

where

$$C_{fw} \equiv 2/U_1^2 \tag{1.3}$$

$$B \equiv \frac{1}{2}\left\{\frac{1}{\gamma-1} + \left(1 - \frac{T_w}{T_0}\right)g + \frac{T_w}{T_0}\left[1 + \frac{D(u_1)}{R_\theta}\right]\right\} \tag{1.4}$$

$$W \equiv \left(\frac{T_0}{T_w}\right)^2 \frac{R_{e*}}{2a(\gamma-1)} K^{\frac{1-2s}{2s}} \tag{1.5}$$

$$b \equiv \frac{1+2s(1-2\gamma)}{2s(\gamma-1)} \tag{1.6}$$

Equations (1.1) and (1.2) constitute two equations for R_θ and g. The coupling appears through the parameter B which contains g. Steczkowski (1969) considered the case $T_w/T_0=1$ and thus analyzed only equation (1.1), which does not depend on g when $T_w/T_0=1$. (Several algebraic errors appeared in Steczkowski's solution. These are corrected in the present analysis.)

Numerical integration of equations (5.17) and (5.18) in Section II shows that the parameter g remains nearly constant for large Mach numbers and is very close to zero. Thus it is fruitful to examine equation (1.1) under the assumption that g is so slowly varying that it can be regarded as constant. The numerical solutions will be discussed later.

A special exact solution to equation (1.1) exists when $\frac{dR_\theta}{dz}=0$. This situation occurs when b=-1. In this case we have

$$\frac{2R_\theta}{C_{fw}} = \frac{W}{\beta} = \text{constant} \qquad (1.7)$$

Because R_θ is an explicit function of C_{fw} , equation (1.7) constitutes an explicit relation for C_{fw}. The value of R_θ can be determined after C_{fw} is known. This equation thus determines the value of R_θ or C_{fw} as a function of W, which is proportional to (T_0/T_w) and the Reynolds number Re , and inversely proportional to the initial expansion angle a. The nozzle shape that corresponds to b=-1 is determined by means of (1.6), that is,

$$s = 1/2\gamma \qquad (1.8)$$

This nozzle expands considerably slower than a cone. The boundary layer may be either laminar-like or turbulent-like in behavior, depending on the value of W. The laminar limit corresponds to $W \rightarrow 0$ and the turbulent behavior occurs for large value of W.

Consider now a more general approximate solution. Following Steczkowski, we assume that the friction coefficient varies as some power of R_θ, that is we assume that $C_{f_W} R_\theta^m = E = \text{constant}$, where m varies in the range $0 < m \leq 1$. More precisely, we assume that m and E vary so slowly that they can be treated as constants in the integration of equation (1.1). Multiplying equation (1.1) by $(1+m)R_\theta^m$ gives

$$\frac{dR_\theta^{1+m}}{dZ} + \frac{(1+m)B}{Z} R_\theta^{1+m} = (1+m)\frac{WE}{Z} Z^{-b} \tag{1.9}$$

If m, E, and B are treated as constants, this equation can be integrated by means of an integrating factor. We get

$$R_\theta^{1+m} = Z^{-(1+m)B}\left\{\frac{(1+m)WE\,Z^{b+1+(1+m)B}}{2[b+1+(1+m)B]} + C_1\right\} \tag{1.10}$$

where C_1 is a constant of integration. We now limit ourselves to the case

$$b + 1 + (1+m)B > 0 \tag{1.10a}$$

For this case the constant of integration can be neglected when $Z \to \infty$, and we get the asymptotic approximation

$$R_\theta^{1+m} = \frac{(1+m) W E Z^{b+1}}{2[b+1+(1+m)B]} \tag{1.11}$$

Now accounting for $E = C_{fw} R_\theta^m$, we can rearrange equation (1.11) to read

$$\frac{2 R_\theta}{C_{fw}} \frac{b+1+(1+m)B}{1+m} = W Z^{1+b} \tag{1.12}$$

This is a general approximation and reduces to expression (1.7) when $b = -1$. This approximation is analogous to that of Steczkowski and depends on the parameter m, which varies in the range $0 < m \leq 1$.

Expression (1.12) describes how R_θ, or C_{fw}, grows or decays with Z, or the Mach number. The nature of the boundary-layer growth as $Z \to \infty$ depends on whether the combination $(b+1)$ is greater or less than zero. When $(b+1) > 0$, the right-hand side of equation (1.12) increases as Z (or M_1) increases. As can be determined by means of equation (1.6), this case corresponds to nozzle shapes such that

$$s < 1/2\gamma \tag{1.13}$$

It follows that R_θ increases with Mach number (or distance downstream in the nozzle) and C_{fw} decreases. This corresponds to a completely turbulent boundary layer. When $(b+1) < 0$, the right-hand side of equation (1.12) decreases as Z (or M_1) increases. The nozzle shapes for this case obey the relation

$$s > 1/2\gamma \tag{1.14}$$

For these nozzle shapes, R_θ decreases with Mach number and C_{fw} increases. This corresponds to a smooth transition from turbulent to laminar flow according to the model of behavior postulated for this analysis. Thus, depending on the nozzle shapes, which govern the pressure gradient, the behavior of the boundary layer can differ substantially.

The displacement thickness can be found by means of expression (6.3) of Section II. We get

$$\frac{\delta^*}{R_{eff}} = \frac{T_w}{T_0}\left\{\left(1-\frac{T_w}{T_0}\right)g + \frac{T_w}{T_0}\left[1+\frac{D(\omega_1)}{R_\theta}\right]\right\}\frac{R_\theta}{R_{e*}}A_e^{1/2}Z \tag{1.15}$$

Use of the asymptotic value of $A_e^{\frac{1}{2}}$ as $Z \rightarrow \infty$ gives

$$\frac{\delta^*}{R_{eff}} = \frac{T_w}{T_0}\left\{\left(1-\frac{T_w}{T_0}\right)g + \frac{T_w}{T_0}\left[1+\frac{D(\omega_1)}{R_\theta}\right]\right\}\frac{R_\theta}{R_{e*}}K^{1/2}Z^{\frac{2\gamma-1}{2(\gamma-1)}} \tag{1.16}$$

One now solves for the variation of R_θ with Z from equation (1.12) and substitutes into equation (1.16) to determine the total variation of δ^*/R_{eff} with Z.

The so-called laminar limit for the above expressions can be found by setting

$$C_{fw} = C_0 C R^{-1}, \quad m=1 \tag{1.17}$$

where

$$C_0 = 1/3 \quad \text{Model A, } U_1 \to 0$$
$$= 8/15 \quad \text{Model B, } U_1 \to 0$$

Equation (1.12) now yields

$$R_\theta = \left(\frac{C_0 C W}{b+1+2B}\right)^{1/2} Z^{\frac{1+b}{2}} \tag{1.18}$$

From equation (1.16), we now obtain

$$\frac{\delta^*}{R_{eff}} = \frac{K^{1/2}}{R_{e*}}\left(2B - \frac{1}{\gamma-1}\right)\left(\frac{C_0 C W}{b+1+2B}\right)^{1/2} Z^{\frac{2\gamma-1}{2(\gamma-1)} + \frac{1+b}{2}} \tag{1.19}$$

The factor D(U)/R that appears in B has the values

$$D(U_1)/R = 3 \quad \text{Model A, } U_1 \to 0$$
$$= 5/2 \quad \text{Model B, } U_1 \to 0$$

The approximate expressions derived in this section illustrate the qualitative behavior of the boundary-layer growth. In the next section, the numerical integration of the differential equations will be discussed. A discussion of the results and a comparison with experiment will then be presented.

2. Numerical Solutions

The differential equations (5.17) and (5.18) in Section II were integrated by means of the Runge-Kutta method. In order to simplify the calculations and reduce the computing time on the digital computer, the asymptotic values of $D(U_1)/R_\theta = 1$ and $E(U_1)/R_\theta = 1$ were utilized. These values are valid when R goes to infinity, or, more practically, when $\kappa U_1 > 10$, as can be seen from Figures 4 and 5. Thus, these approximations are appropriate for turbulent flow. For laminar-like behavior, these approximations will produce a displacement thickness that is too high. This can be seen from equation (1.18), wherein the factor (b+1+2B) becomes too small, since (b+1) is negative for laminar-like flow and B is smaller than it should be because of the above approximation for $D(U_1)/R_\theta$. Nevertheless, the correct qualitative behavior is obtained and the simplifications were thus felt to be justified.

In order to carry out the integrations, initial conditions had to be assumed. It was found that the flow far downstream was independent of the initial conditions, which corresponded to a thin boundary layer at the throat of the nozzle. Some of the calculations showing the effect of the initial conditions are shown in Figures 6-9. In these calculations , the common conditions were $=1.4$, $R_{e*}=64\times10^4$, $T_w/T_0=1/3$, and an initial expansion angle $a=4^{\circ}$. Two nozzle shapes were selected: s=1, a conical nozzle for which the boundary layer remains laminar-like; and s=1/3 for which the boundary layer remains turbulent throughout the nozzle. The assumed initial values of C_{fwt} and g_t , which corresponds to $\xi=0$ and $M_1=1$, and the assumed values of T_w/T_0 for the different values of s and the two stress models are summarized in the following table.

Table I

Figure	C_{fwt}	g_t	s	Shear Stress Model
6	0.0036	0.75	1	A,B
7	0.0040	0.50	1/3	A
7	0.0020	0.75	1/3	A
8	0.0036	0.50	1/3	A
8	0.0036	0.50	1	A
9	0.0036	0.50	1/3	B
9	0.0036	0.50	1	B

Figure 6 compares Model A and B under the same flow conditions. The general trend for the variations of C_{fw}, R_θ, and g with Mach number is the same, and there is very little difference between the two models. The variable g becomes nearly zero when $M_1 > 10$ for this conical nozzle case. The boundary layer is becoming laminar-like with increasing Mach number.

Figure 7 illustrates the small effect of initial conditions (imposed at the throat) on the flow far downstream in the nozzle. Two sets of calculations for $C_{fwt}=0.0040$ and $g_t=0.50$ and for $C_{fwt}=0.0020$ and $g_t=0.75$ produce almost identical results far downstream. These results were obtained for Model A, but it is expected that similar behavior would result for Model B.

Figures 8 and 9 show the differences in boundary-layer behavior that result because of nozzle shape. The results for Model A (Fig.8) and Model B (Fig.9) are qualitatively the same. For a conical nozzle, s=1, the boundary layer tends to become laminar-like, as was predicted by the asymptotic approximations. For s=1/3, which is less than the critical value s=1/2 predicted by the asymptotic approximation, the boundary-layer remains turbulent and does not revert to a laminar-like behavior. Thus the numerical results substantiate the asymptotic approximations. For both nozzle shapes, the variable g becomes small and tends toward a constant value as Mach number increases.

Figures 10 to 13 show the trends of displacement-area growth for the flow conditions associated with Figures 8 and 9. The faster growth for turbulent flow is illustrated as expected.

Figures 14 to 17 show the velocity and density profiles at M =8 and 16 for the flow conditions associated with Figure 7. The general pattern of the velocity and density distributions and their development along the flow are shown.

3. Comparison with Experiment

In this section we shall compare the results of the present analysis with the experimental data of Kemp and Sreekanth (1969). The nozzle for these experiments was a contour nozzle that aorrelated approximately with values $a=7^{o}$ and $s=0.79$. The working gas was Helium ($\gamma=5/3$), the Reynolds numbers were in the range $2x10^5 \leq R_{e_*} \leq 1.8x10^6$, and the wall temperature ratios were in the range $0.35 \leq T_W/T_0 \leq 0.70$. The displacement-thickness data as a function of Mach number are listed in Table II and plotted in Figure 18.

TableII

M_1	27.0	26.4	27.9	27.6	28.6	29.3	
$\delta^{(t)}/R$	0.34	0.35	0.33	0.28	0.29	0.27	
M_1	29.4	32.2	36.8	45.5	44.6	47.0	47.3
$\delta^{(t)}/R$	0.26	0.38	0.47	0.49	0.51	0.48	0.51

Also shown in Figure 18 are the results of the numerical integration of equations (5.17) and (5.18). The Reynolds number and wall temperature used for these calculations are $R_{e_*}=10^6$ and $T_w/T_0=1/3$, which are representative values corresponding to the data of Kemp and Sreekanth. In addition, a linear viscosity law was used with C=1. The results shown are independent of the initial conditions at the throat. For these calculations Model A was used for the velocity profile and the initially turbulent boundary layer is undergoing transition towards a laminar-like behavior (which is consistent with our previous analysis). As one can see from Figure 18, the calculated curve lies significantly above the data of Kemp and Sreekanth.

To better interpret these results, it is useful to introduce the curve that arises from purely laminar flow, that is, equation (1.19) of section III together with equation (6.7) of section II. For simplicity we set g=0 since the numerical solutions showed that this is a good approximation. The purely laminar flow will always have a displacement thickness that is less than that for any degree of turbulent flow under the same conditions. The curve for laminar flow is also plotted in Figure 18. The laminar displacement thickness is smaller at low Mach numbers than that for the thickness arising from the general analysis but is larger at the higher Mach numbers. The too large values at the high Mach numbers arises because of the approximation g=0 for the laminar curve. The displacement thicknesses for both of the theoretical calculations are significantly larger than the experimental data.

There are several possible explanations for the disagreement between the theory and experiment. It does appear that the flow in the nozzle has undergone transition from a completely turbulent behavior toward a behavior that has a more laminar-like behavior. Any completely turbulent velocity profile would produce displacement thicknesses that are greater than the theoretical values shown in Figure 18. Thus the velocity profile model developed for the theoretical analysis does not seem to be the main cause of the discrepancy.

It is useful to consider what parameters can be varied in the theoretical analysis in order to produce a significantly small displacement thickness. In this regard the laminar formula (1.19) of section III is useful. Since the Reynolds number, wall temperature, nozzle shape, and the ratio of specific heats $\gamma=5/3$ are specified by the experimental conditions, these parameters are more or less fixed. The parameter that can be examined more closely is the parameter C in the viscosity law, which was set equal to unity in the previous calculations. The parameter C was defined in equation (2.11) as

$$C \equiv \left[\sqrt{\frac{T}{T_w}} \quad \frac{T_w + S}{T + S}\right]_{\text{average}}$$

This parameter thus represents some average value across the boundary layer. Because the temperature of the inviscid core flow is exceedingly small for very large Mach numbers, the value of C corresponds to some average temperature between the free stream and wall temperatures. It follows that C will have some value between zero and unity. In Figure 18, the laminar curves for displacement thickness have been drawn for arbitrary values of C=1, 0.4, and 0.2. Better agreement is obtained with the data when C is selected to be 0.2. It thus appears that because of the large temperature change across the boundary layer the precise variation of viscosity with temperature should be taken into account.

Another comparison of experiment with the present analysis can be made with the velocity profile and density profile as determined by Kemp and Sreekanth. These data, corresponding to the previous data for displacement thickness, are shown in Figures 19 and 20 for M_1=44.6. For comparison the curves corresponding to the numerically integrated solutions are also shown. At M_1=44, the Reynolds number from the numerical solution is 130 which implies a laminar-like flow. It is seen from these figures that the theoretical velocity profile is in fair agreement with the experimental data. The biggest discrepancy occurs at the outer edge of the boundary layer, which would be expected since Model A is least valid in this region. The comparison for the density profile is not good because this also corresponds to the outer edge of the boundary layer.

IV DISCUSSION AND CONCLUDING REMARKS

The turbulent boundary-layer development far downstream in a slender hypersonic nozzle has been examined by means of integral methods. Heat transfer, boundary-layer displacement, and transverse curvature have been taken into account. The most important approximations were those involving the velocity and enthalpy profiles. These approximations were in accordance, however, with known special cases of boundary-layer behavior. It is thus expected that the extrapolation to the new regime of hypersonic nozzle flow would predict at least qualitatively the essential behavior of this type of flow.

As pointed out by Patel and Heaf (1968), the usual law-of-the wall profile must be modified by means of a pressure-gradient parameter when strong pressure gradients are present. Although various possibilities were discussed by them, it is not clear how the pressure-gradient parameter would enter explicitly into the velocity-profile representation. This is particularly true when the compressible flow in a hypersonic nozzle is considered. In this investigation it was assumed implicitly that the pressure gradient affects the boundary-layer growth essentially through the momentum-integral equation. The direct effect of the pressure-gradient on the velocity profile is thus assumed to be of secondary importance. This assumption is in accordance with the general result that the boundary-layer growth predicted by the integral form of the boundary-layer equations is relatively insensitive to the details of the velocity profile.

The relaminarization of the boundary layer in the present analysis is governed by the relative thickness of the viscous sublayer. Whereas the pressure gradient is not included explicitly in the velocity profile, the viscous sublayer is. As the viscous sublayer comprises a larger percentage of the boundary-layer thickness, the boundary layer is regarded as behaving more laminar-like. Because the momentum thickness governs the relative extent of the viscous sublayer, the momentum-integral equation, which governs the momentum thickness, determines the extent to which the boundary layer behaves laminar-like. It follows, therefore, that the pressure gradient affects the velocity profile indirectly by means of the momentum-integral equation. The models for the velocity profile in this analysis thus allow for a smooth transition from turbulent to laminar-like flow--relaminarization--in terms of the variation of the momentum-thickness Reynolds number.

When the above premises are adopted and approximate and numerical solutions to the integral forms of the equations obtained for hypersonic flow in a slowly expanding nozzle, it is discovered that reverse transition from turbulent to laminar-like flow is obtained for certain nozzle shapes. The present models thus are capable of predicting reverse transition. These findings agree qualitatively with the hypothetical flow of Kline (1967) constructed to illustrate his observed features of relaminarization.

The quantitative aspects of the present investigation were compared with the experimental data of Kemp and Sreekanth (1969). The theoretical displacement thickness was found to be larger than the experimental. Because a more laminar-like boundary layer will have a small displacement thickness, this is an indication that the flow was in a transition toward a laminar-like behavior. Part of the discrepancy between theory and experiment can be attrbuted to the linear viscosity-temperature law used in the calculations. As was pointed out earlier, because of the great temperature change across the hypersonic boundary layer, a more exact viscosity law would be preferred for precise calculations.

The present analysis is suitable as a framework for further investigation. It can be used for a parametric study on the effects of such parameters as nozzle shapes, wall temperature ratio, and reservoir conditions. In this regard, it would be useful to have more experimental data available for comparison. Finally, a methodology has been suggested for analyzing hypersonic nozzle flow problems.

REFERENCES

Bucknell, D.M. & Beckwith, I. E. (1970). "Calculation of Non-equilibrium Hypersonic Turbulent Boundary Layer and Comparison with Experimental Data", AIAA J., Vol.8, No.8, August, pp.1462-1469.

Coles, D. (1964). "Turbulent Boundary Layer in Compressible Fluids", Physics of Fluids, Vol.7, No.9, p.1403.

Kemp, J. H. & Sreekanth, A. K. (1969). "Preliminary Results from an Experimental Investigation of Nozzle Wall Boundary Layers at Mach Numbers Ranging from 27 to 47", AIAA paper No.69-686, AIAA 2nd Fluid and Plasma Dynamics Conference, San Francisco, June 16-18.

Kline, S. J. (1967). "Observed Structure Features in Turbulent and Transitional Boundary Layers", Fluid Mechanics of Internal Flow, Elsevior Publishing Co., pp.27-79.

Laufer, J. (1969). "On Turbulent Shear Flows of Variable Density", AIAA J., Vol.7, No.4, pp.706-713.

Lewis, J. E., Kubota, T., & Webb, W. H. (1970). "Transformation Theory for the Adiabatic Compressible Turbulent Boundary Layer with Pressure Gradient", AIAA J., Vol.8, No.9, September, pp.1644-1650.

Liepmann, H. W. & Roshko, A. (1958). Elements of Gasdynamics, Galcit Aeronautical Series, John Wiley & Sons, Inc.

Mager, A. (1958). "Transformation of the Compressible Turbulent Boundary Layer", JAS, Vol.25, No.5, pp.305-311.

Maise, G. & McDonald, H. (1968). "Mixing Length and Kinematic Viscosity in a Compressible Boundary Layer", AIAA J., Vol.6, No.1, pp.73-80.

Patel, V. C. & Head, M. R. (1968). "Reversion of Turbulent to Laminar Flow", J. of Fluid Mechanics, Vol.34, p.371.

Rasmussen, M. L. & Karamcheti, (1966). "Viscous Effects Far Downstream in a Slowly Expanding Hypersonic Nozzle", AIAA J. Vol.4, No.5, May, pp.807-815.

Rasmussen, M. L. & Karamcheti, (1965). "On the Viscous Sublayer of an Incompressible Turbulent Boundary Layer", Stanford University SUDAER No.219, February.

Rasmussen, M. L. & Karamcheti, (1964). "An Analytic Study of Viscous Effects in a Slowly Expanding Hypersonic Nozzle", Stanford University SUDAER No.186, April.

Schlichting, H. (1964). <u>Boundary Layer Theory</u>, McGraw Hill Series in Mechanical Engineering.

Senoo, Y. (1957). "The Boundary Layer on the End Wall of a Turbine Nozzle Cascade", MIT Gas Turbine Lab. Rept No.35, Also TASME 80, p.1711, and ASME Paper A-172.

Sergienko, A. A. & Gretsov, V. K. (1959). "Transition from a Turbulent into a Laminar Boundary Layer", Soviet Physics Doclady, Vol.4, No.1.

Spalding, D. B. (1961). "A Single Formular for the Law-of-the-Wall", Trans. Amer. Soc. Mechanical Engineering, J. Applied Mechanics 28 Series E, p.455.

Steczkowski, A. F. (1969). "Turbulent Boundary Layer Characteristics Far Downstream in a Slowly Expanding Hypersonic Nozzle", Master of Science Thesis, University of Oklahoma.

Sternberg, J. (1954). "The Transition from a Turbulent to Laminar Boundary Layer", U. S. Army Bal. Res. Lab. Rept.906, Aberdeen, Maryland.

Van Driest, E. R. (1951). "Turbulent Boundary Layer in Compressible Fluids", JAS, Vol.18, pp.145-160.

Williams, J. C. (1963). "A Study of Compressible and Incompressible Flow in Slender Channels", AIAA J., January, p.186.

Wilson, R. E. (1950). "Turbulent Boundary Layer Characteristics at Supersonic Speeds--Theory and Experiment", JAS, Vol.17, No.9, pp.585-594.

APPENDIX I

Some integrals in the analysis involve the derivative

$$\frac{d\eta}{du} = 1 + \frac{2\kappa}{\beta}(\sinh \kappa u - \kappa u)$$

A few of them can be integrated in closed form as follows:

$$a = \int_0^u \left[1 + \frac{2\kappa}{\beta}(\sinh \kappa u - \kappa u)\right] du$$

$$= u + \left[\frac{2}{\beta}\left(\cosh \kappa u - \frac{(\kappa u)^2}{2} - 1\right)\right]$$

$$b = \int_0^u \frac{u}{u_1}\left[1 + \frac{2\kappa}{\beta}(\sinh \kappa u - \kappa u)\right] du$$

$$= \frac{u^2}{2u_1} + \frac{2}{\beta}\left[\frac{u}{u_1}\cosh \kappa u - \frac{\sinh \kappa u}{\kappa u_1} - \frac{u}{u_1}\frac{(\kappa u)^2}{3}\right]$$

$$c = \int_c^u \left(\frac{u}{u_1}\right)^2\left[1 + \frac{2\kappa}{\beta}(\sinh \kappa u - \kappa u)\right] du$$

$$= \frac{u^3}{3u_1^2} + \frac{2}{\beta}\left[\left(\frac{u}{u_1}\right)^2\cosh \kappa u - \frac{2u}{u_1}\frac{\sinh \kappa u}{\kappa u_1} - \frac{2(\cosh \kappa u - 1)}{(\kappa u_1)^2}\right.$$

$$\left. - \left(\frac{u}{u_1}\right)^2\frac{(\kappa u)^2}{4}\right]$$

$$d = \int_0^u \left[\left(\frac{u}{u_1}\right)^3\left[1 + \frac{2\kappa}{\beta}(\sinh \kappa u - \kappa u)\right]\right] du$$

$$= \frac{u^4}{4u_1^3} + \frac{2}{\beta}\left[\left(\frac{u}{u_1}\right)^2 \cosh \kappa u - \frac{3u^2}{u_1^2}\frac{\sinh \kappa u}{\kappa u_1} + \frac{6u}{u_1}\frac{\cosh \kappa u}{(\kappa u_1)^2} - \frac{6\sinh \kappa u}{(\kappa u_1)^3} - \frac{\kappa^2 u^5}{5\, u_1^3} \right]$$

Thus in ((3.2) II)

$$\int_0^{u_1} u\left(1-\frac{u}{u_1}\right)\frac{d\eta}{du}\,du = u_1(b-c)_{u=u_1}$$

in ((3.18) II)

$$\int_0^{u_1} u\,\frac{u}{u_1}\left(1-\frac{u}{u_1}\right)\frac{d\eta}{du}\,du = u_1(c-d)_{u=u_1}$$

in ((3.26) II)

$$\int_0^{u_1}\left(1-\frac{u}{u_1}\right)\frac{d\eta}{du}\,du = (a-u_1 b)_{u=u_1}$$

and in ((4.6) II)

$$\int_0^{u_1}\left[\frac{T_0}{T_w}\frac{1}{Z}\left(\frac{u}{u_1}\right)^2 + 1 - \left(\frac{u}{u_1}\right)^2 + \left(\frac{T_0}{T_w}-1\right) g\,\frac{u}{u_1}\left(1-\frac{u}{u_1}\right)\right]\frac{d\eta}{du}\,du$$

$$= \left[\frac{T_0}{T_w}\frac{1}{Z}\,c - a - c + \left(\frac{T_0}{T_w}-1\right) g\,(b-c)\right]_{u=u_1}$$

APPENDIX II

The derivative of the nozzle longitudinal axis ξ with respect to the flow variable Z is one of the key variables to higher approximations. Rasmussen and Karamcheti (1964) obtained in the notation of this paper the expression

$$\frac{d\xi}{dZ} = \frac{\frac{d\ln A_e}{dZ} + \frac{2\theta}{R}\left[\frac{d}{dZ}\left(\frac{\delta^*}{\theta}\right) - \frac{\delta^*}{\theta}\left(1+\frac{\delta^*}{\theta}\right)\frac{d\ln u_1}{dZ}\right]}{\frac{d\ln A}{d\xi} - \frac{c_f r_o \delta^*}{R\theta}} \tag{A-1}$$

This study developed the same derivative in another way as shown in ((5.13) II)

$$\frac{d\xi}{dZ} = \frac{1}{2a}\left(\frac{A}{A_e}\right)^{1/2s} A_e^{1/2s}\left[\frac{d\ln(A/A_e)}{dZ} - \frac{d\ln A_e}{dZ}\right] \tag{A-2}$$

These two expressions are basically identical. The proof goes: As is defined in ((5.4) II)

$$A = \left(1+\frac{a}{s}\xi\right)^{2s}$$

differentiating with respect to ξ, one obtains

$$\frac{d\ln A}{d\xi} = \frac{d}{d\xi}\ln\left(1+\frac{a}{s}\xi\right)^{2s} = \frac{2a}{A^{1/2s}} = 2a\Big/\left(\frac{A}{A_e}\right)^{1/2s} A_e^{1/2s} \tag{AII-1}$$

From the equation ((1.15) II), setting Q=1 and differentiating logarithmically with respect to Z, one arrives

$$\frac{d\ln(A/A_e)}{dZ} = -\frac{d}{dZ}\ln\left(1-\frac{2\delta^*}{R}\right) = \frac{2A}{A_e}\frac{d}{dZ}\left(\frac{\delta^*}{R}\right) \tag{AII-2}$$

One notices that

$$\frac{d}{dZ}\left(\frac{\delta^*}{\theta}\right) = \frac{d}{dZ}\left(\frac{\delta^*}{\theta}\frac{\theta}{R}\right) = \frac{\theta}{R}\frac{d}{dZ}\left(\frac{\delta^*}{\theta}\right) - \frac{\delta^*}{\theta}\frac{d\ln R}{dZ} + \frac{\delta^*}{\theta}\frac{d\ln\theta}{dZ} \tag{AII-3}$$

One goes back to ((1.21) II) and deduces

$$\frac{d\ln\theta}{dZ} = \frac{C_f r_*}{2\theta}\frac{d\xi}{dZ} - \frac{d\ln R}{dZ} + \frac{d\ln A_e}{dZ} - \left(1+\frac{\delta^*}{\theta}\right)\frac{d\ln u_1}{dZ} \tag{AII-4}$$

Substituting this expression in (AII-3), one obtains

$$\frac{d}{dZ}\left(\frac{\delta^*}{R}\right) = \frac{\theta}{R}\frac{d}{dZ}\left(\frac{\delta^*}{\theta}\right) + \frac{\delta^*}{R}\frac{d\ln A_e}{dZ} - \left(1+\frac{\delta^*}{\theta}\right)\frac{d\ln u_1}{dZ}$$

$$-\left(\frac{\delta^*}{R}\frac{d\ln A}{d\xi} - \frac{C_f r_* \delta^*}{2R\theta}\right)\frac{d\xi}{dZ} \tag{AII-5}$$

Equation (A-2) can now be rewritten as

$$\frac{d\xi}{dZ}\frac{d\ln A}{d\xi} = \frac{2A}{A_e}\frac{\theta}{R}\frac{d}{dZ}\left(\frac{\delta^*}{\theta}\right) + \frac{\delta^*}{R}\frac{d\ln A_e}{dZ} - \left(1+\frac{\delta^*}{\theta}\right)\frac{d\ln u_1}{dZ}$$

$$-\left(\frac{\delta^*}{R}\frac{d\ln A}{d\xi} - \frac{C_f r_* \delta^*}{2R\theta}\right)\frac{d\xi}{dZ} + \frac{d\ln A_e}{dZ} \tag{AII-6}$$

Rearranging this expression, one writes

$$\left[\frac{d \ln A}{d \xi} + \frac{2A}{A_e}\left(\frac{\delta^*}{R} \frac{d \ln A}{d \xi} - \frac{C_f r_0 \delta^*}{2R\theta} \right) \right] \frac{d \xi}{d Z}$$

$$= \frac{2A}{A_e}\left[\frac{\theta}{R} \frac{d}{dZ}\left(\frac{\delta^*}{\theta} \right) - \frac{\delta^*}{\theta}\left(1 + \frac{\delta^*}{\theta} \right) \frac{d \ln u_1}{d Z} \right] + \left(1 + \frac{A}{2A_e} \frac{\delta^*}{R} \right) \frac{d \ln A_e}{d Z} \qquad \text{(AII-7)}$$

Recalling ((1.15) II) in setting Q=1, we have

$$1 + \frac{2A}{A_e} \frac{\delta^*}{R} = 1 + 2 \frac{\delta^*}{R} \Big/ \left(1 - \frac{2\delta^*}{R} \right) = \left(1 - \frac{2\delta^*}{R} \right)^{-1} = \frac{A}{A_e} \qquad \text{(AII-8)}$$

One concludes that (AII-7) is identical to (A-1).

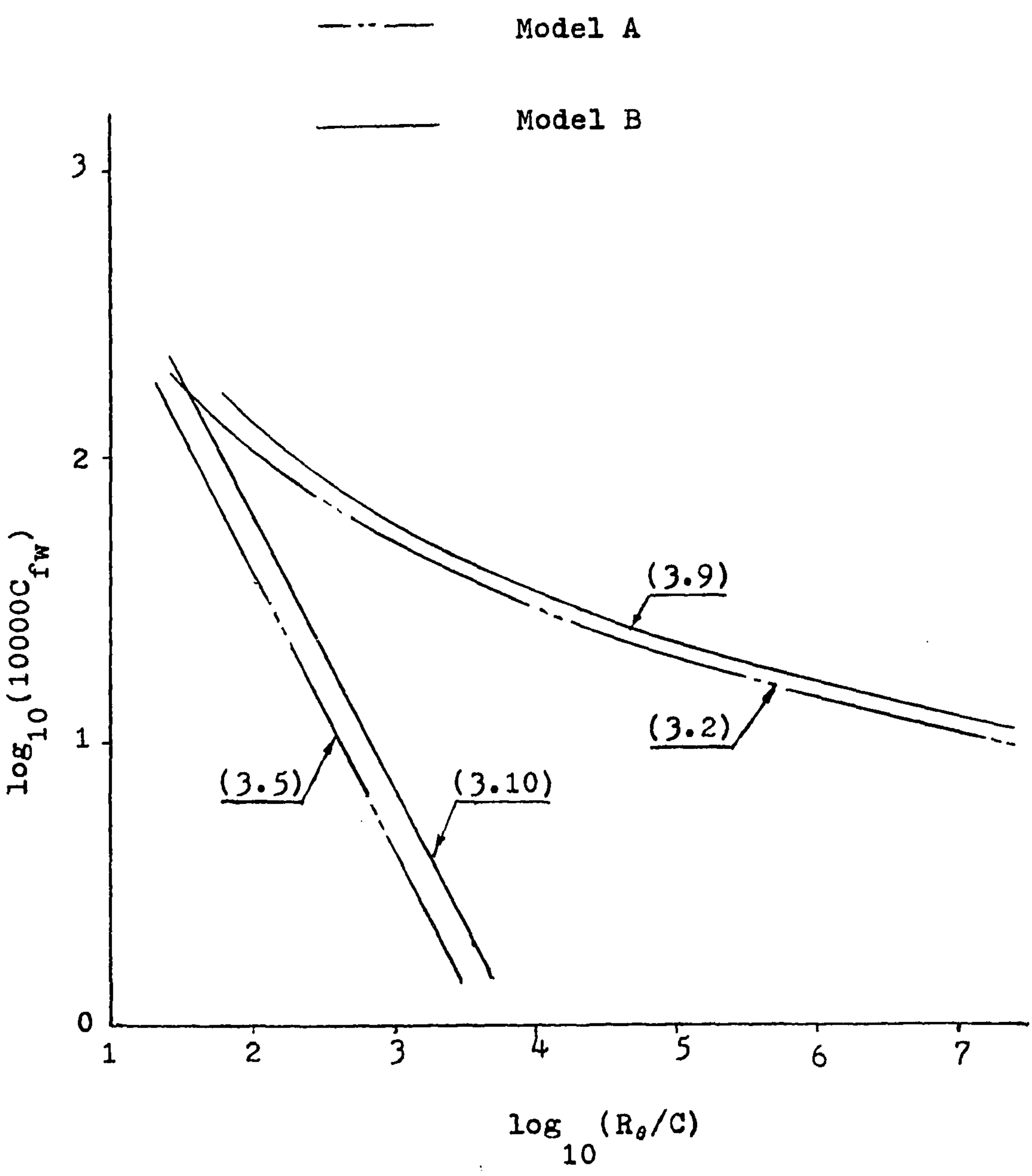

Figure 1. Model A & B: C_{fw} vs. R_θ (C=1).

Model A

C=1

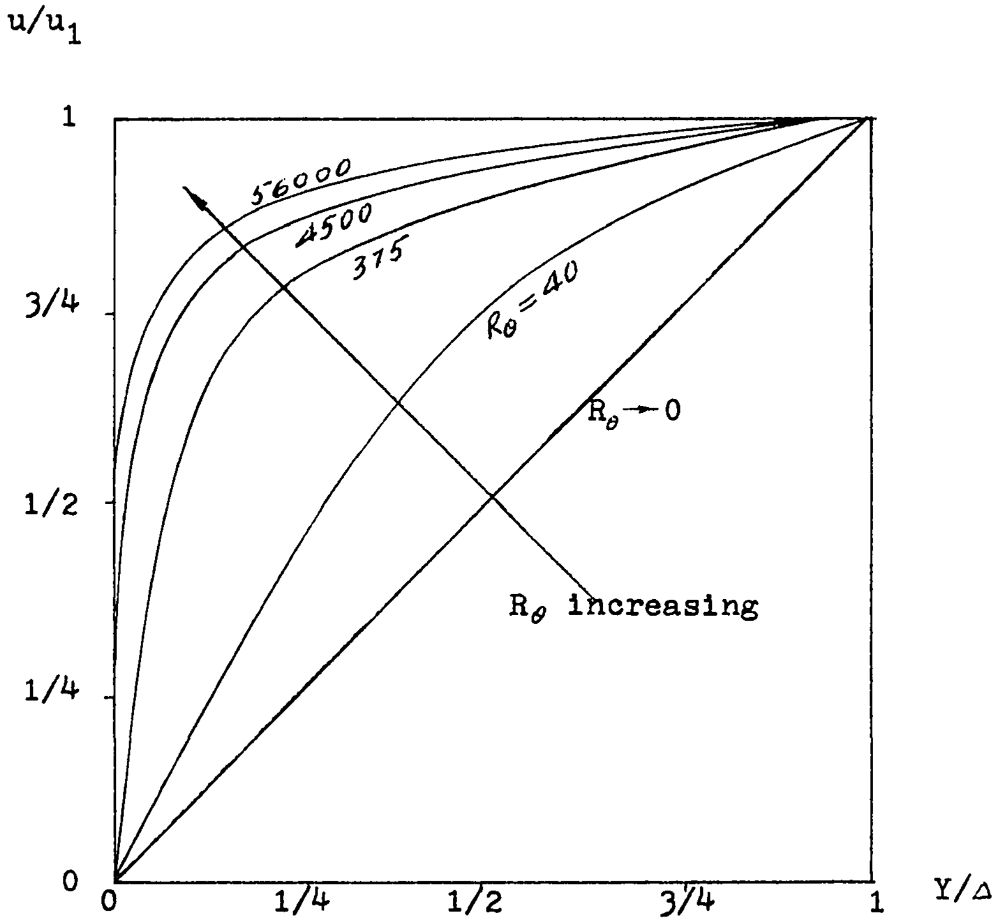

Figure 2. Model A: u/u_1 vs. Y/Δ, Velocity Profiles.

Model B

C=1

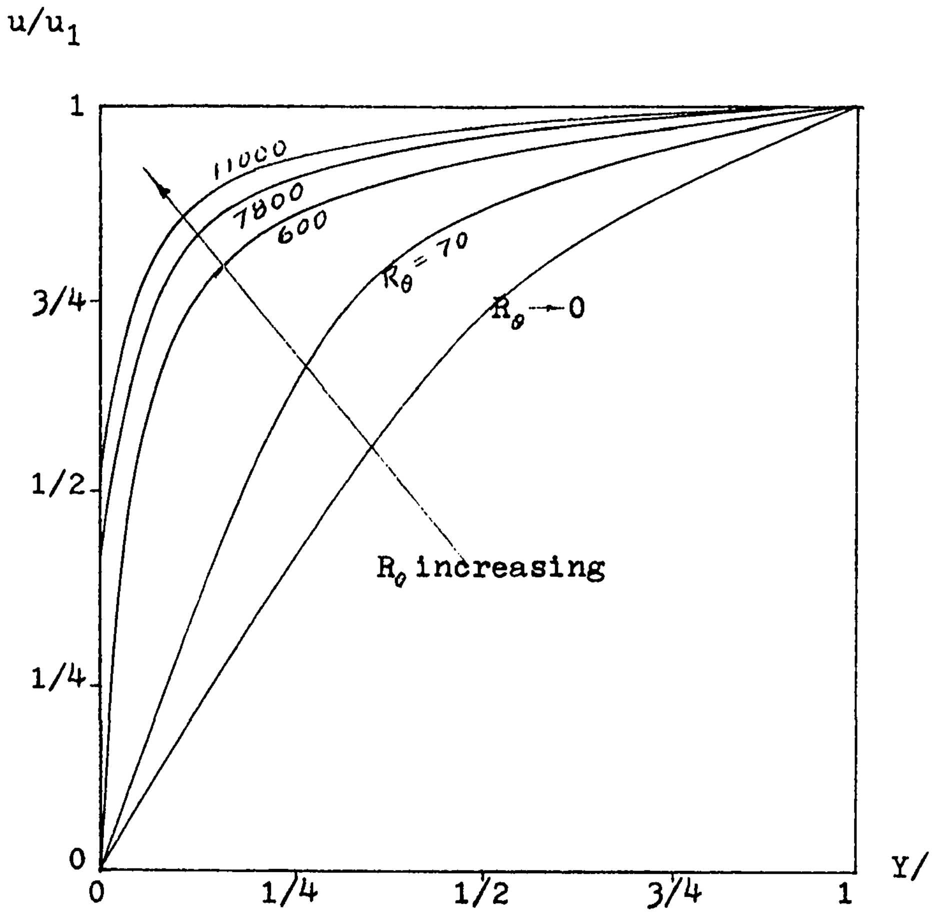

Figure 3. Model B: u/u_1 vs. Y/Δ, Velocity Profiles.

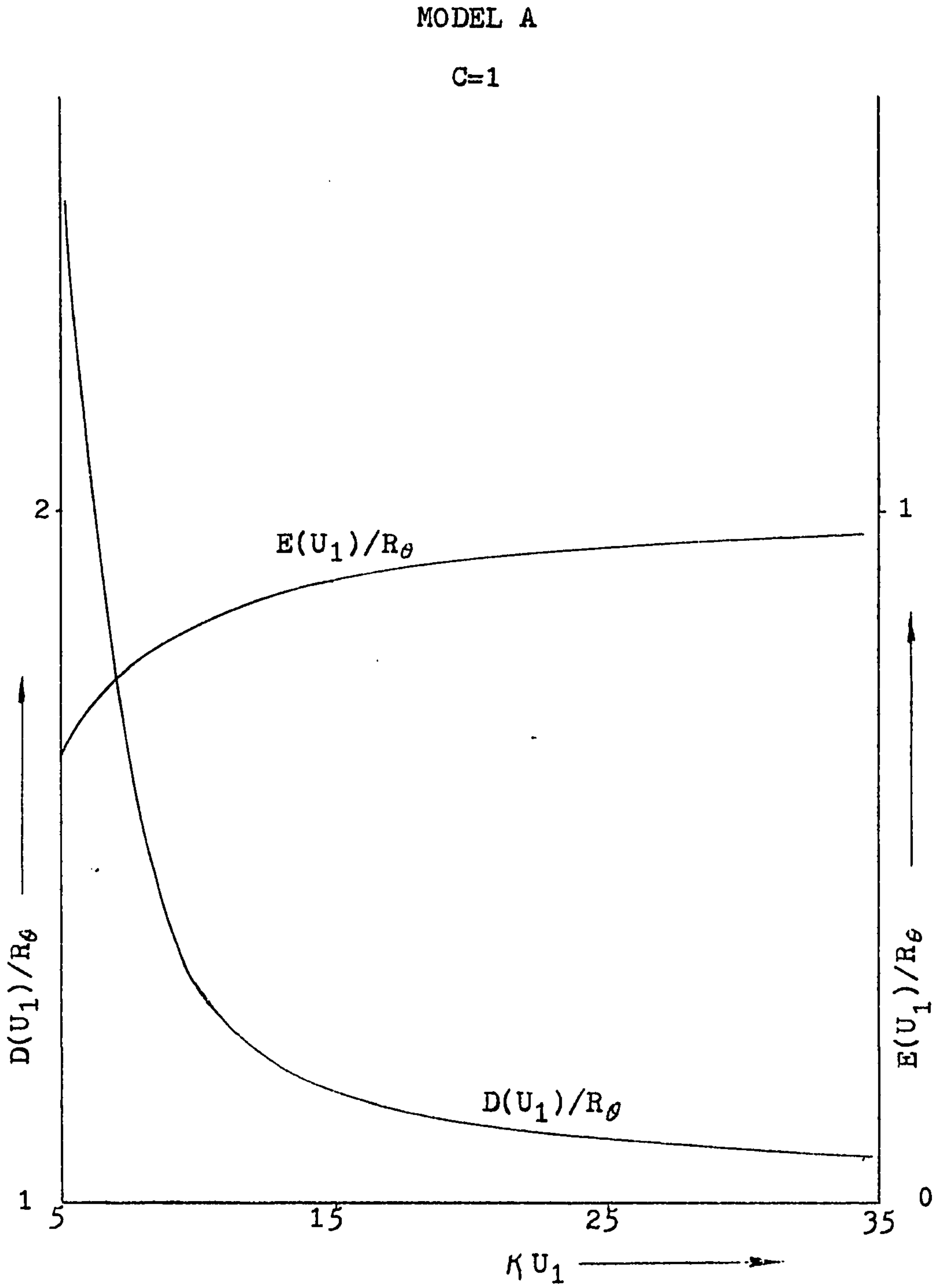

Figure 4. Model A: $D(U_1)/R_\theta$ & $E(U_1)/R_\theta$ vs. κU_1.

MODEL B

C=1

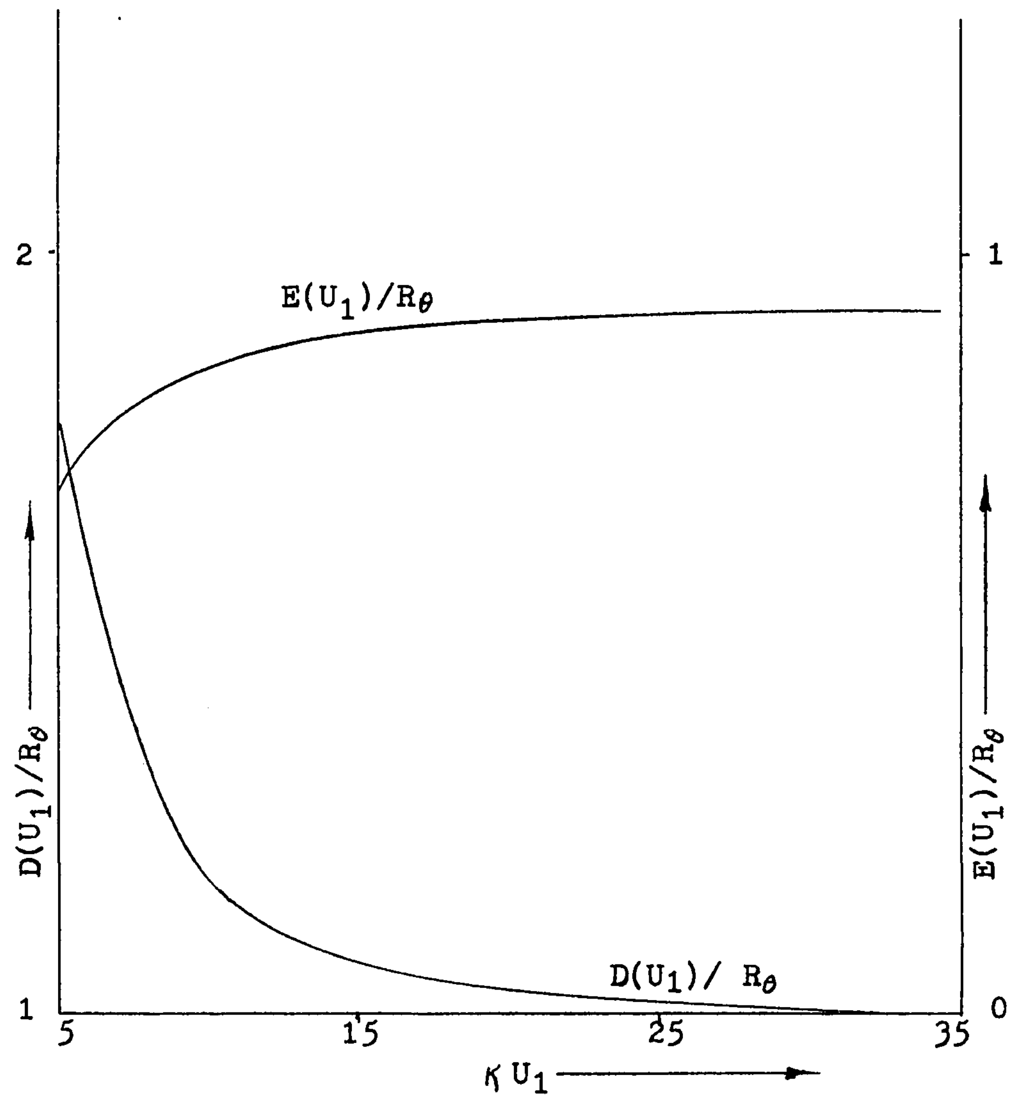

Figure 5. Model B: $D(U_1)/R_\theta$ & $E(U_1)/R_\theta$ vs. κU_1.

73

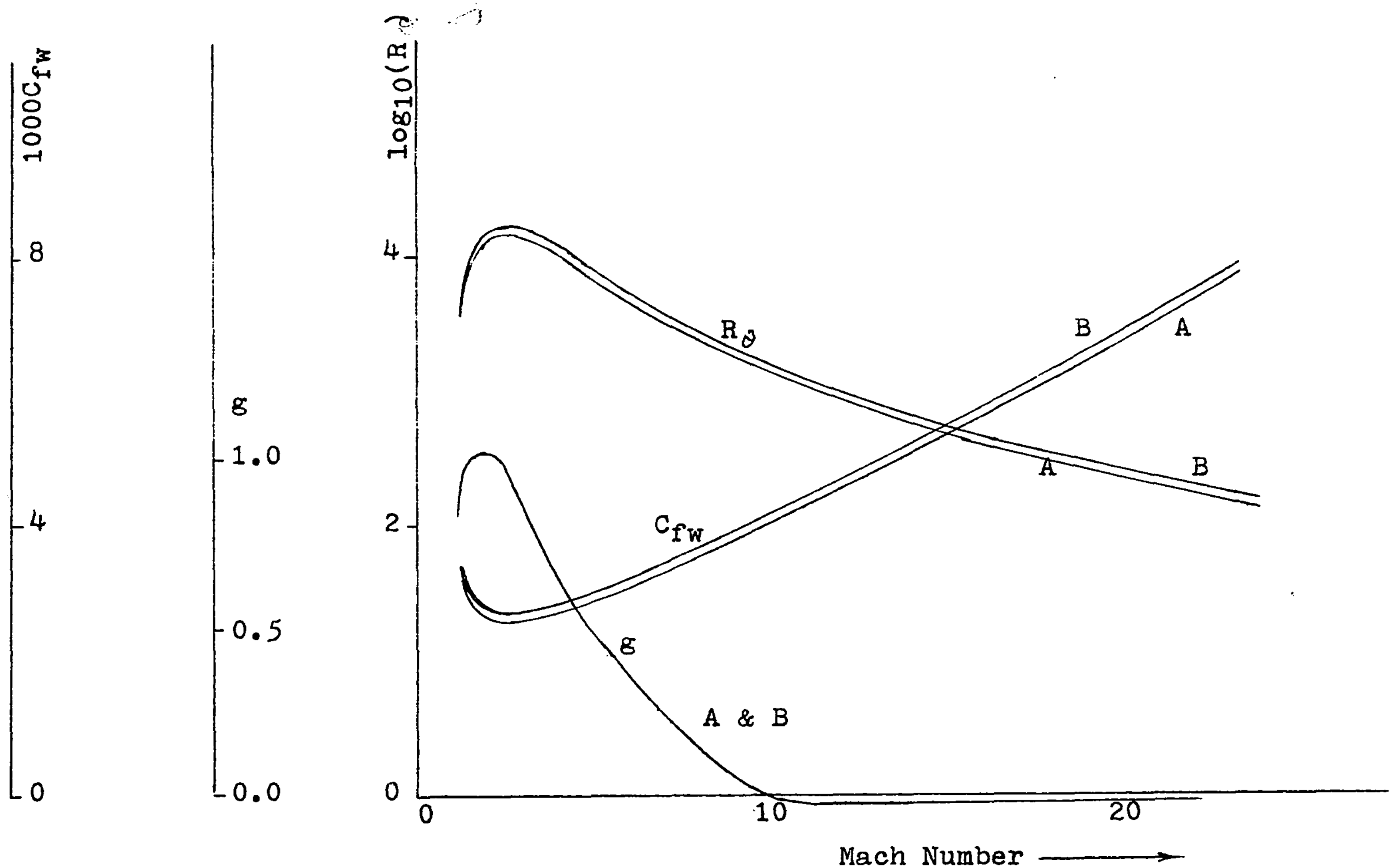

Figure 6. Model A & B: Numerical Solution.

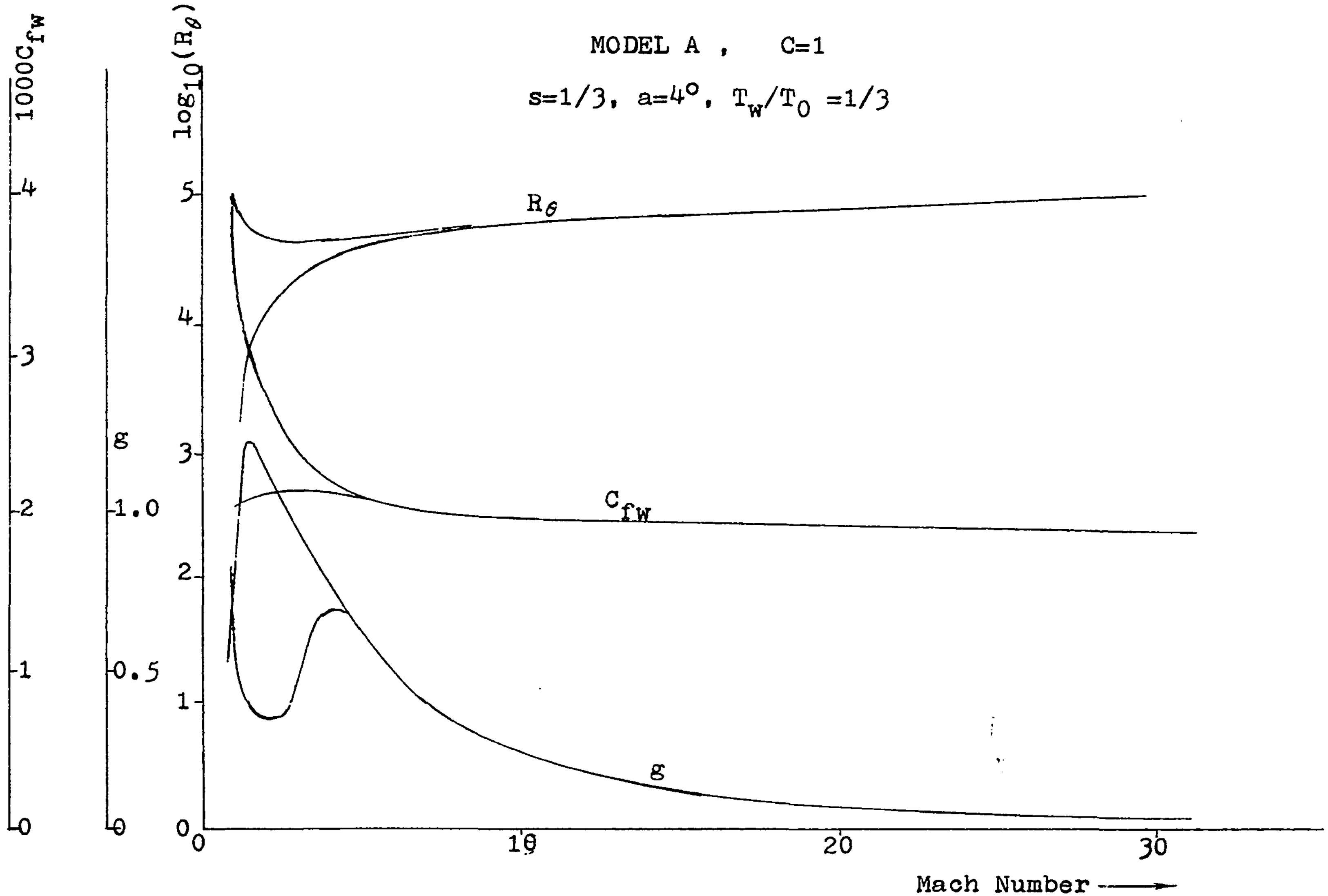

Figure 7. Model A: Numerical Solution.

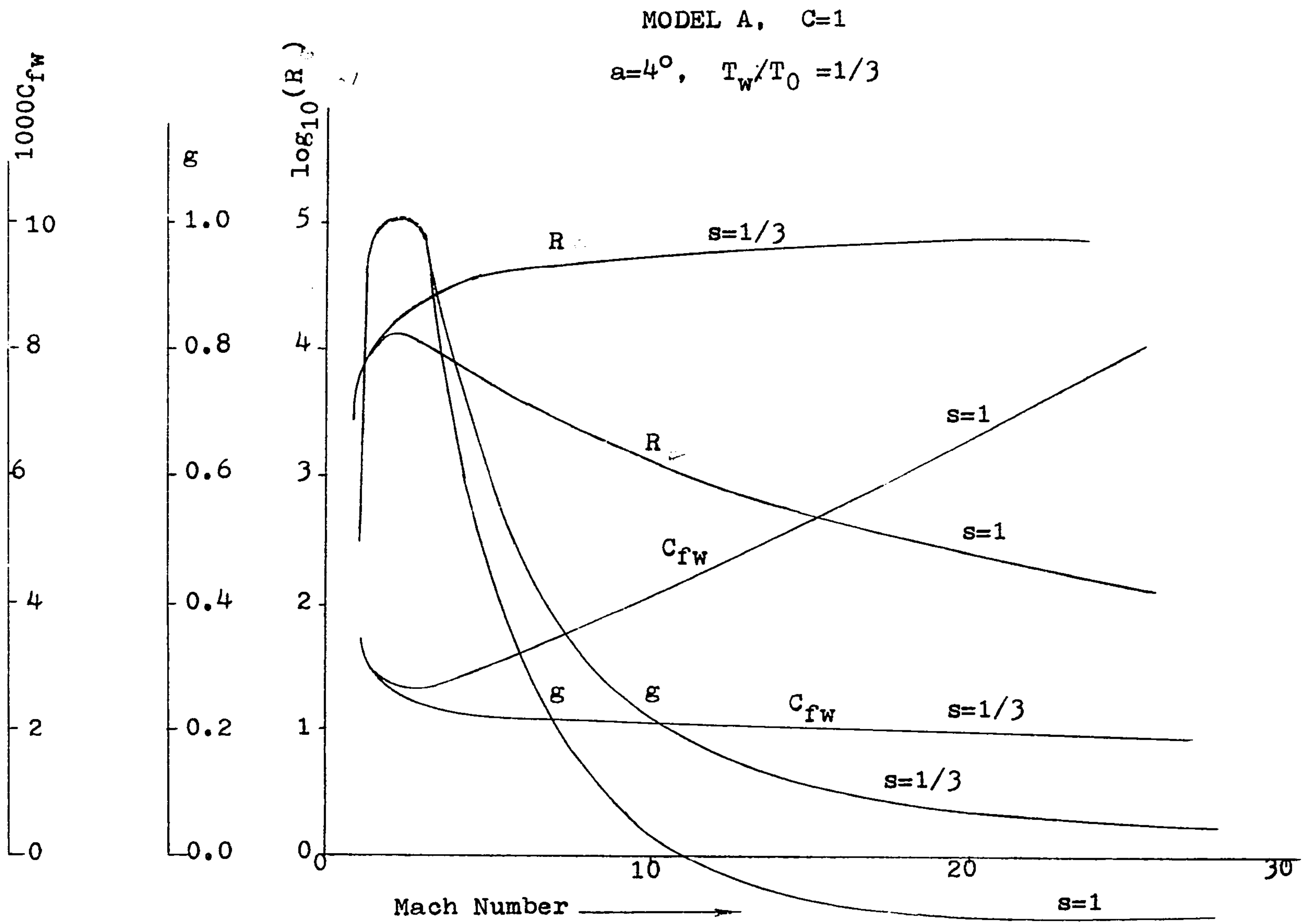

Figure 8. Model B: Numerical Solution.

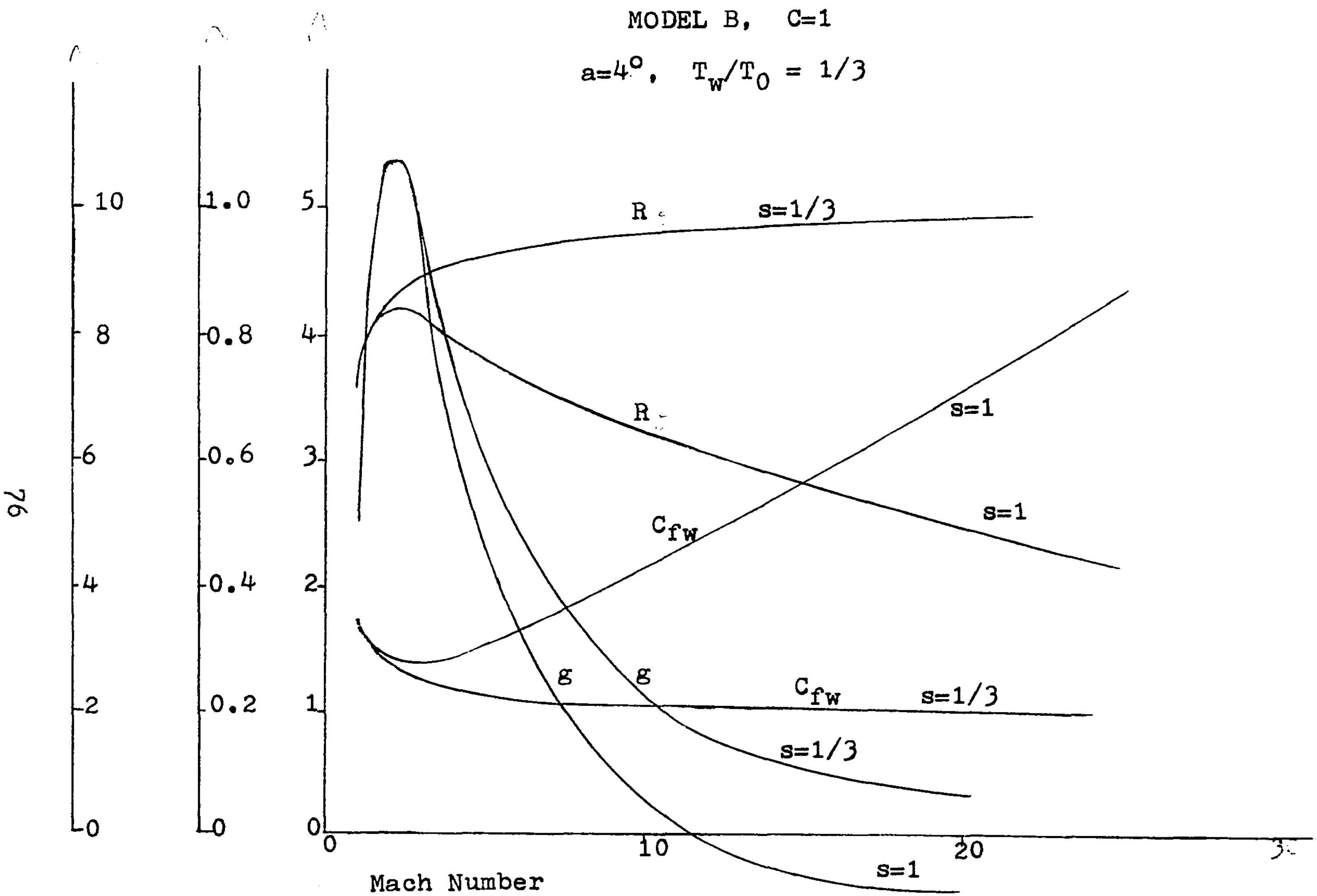

Figure 9. Model B: Numerical Solution.

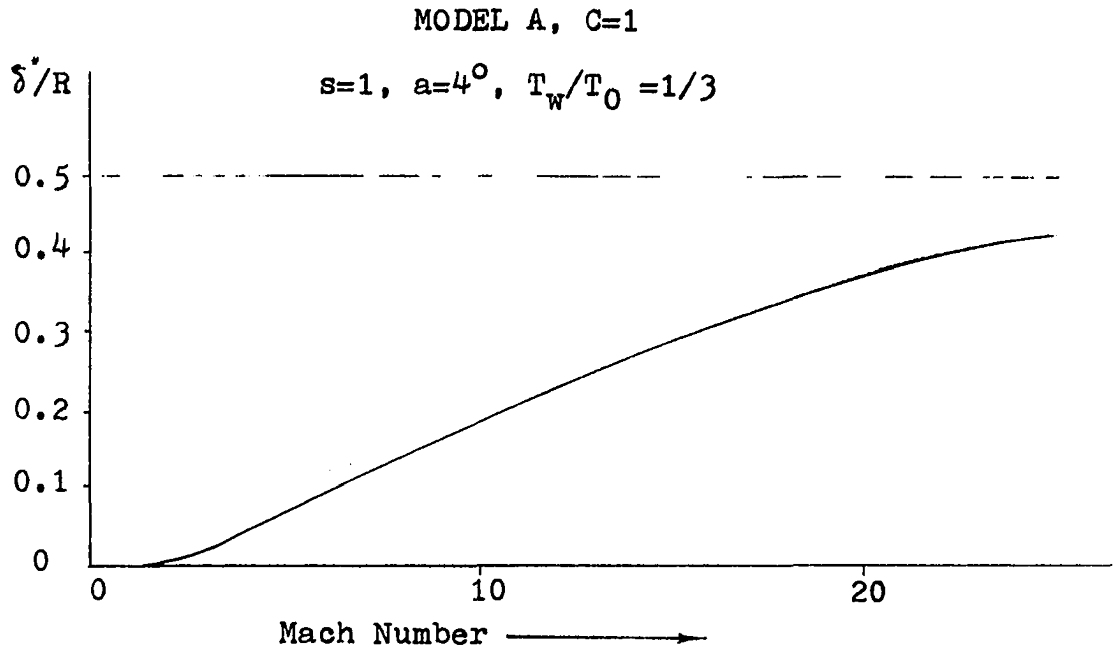

Figure 10. Model A: Displacement-Area Growth.

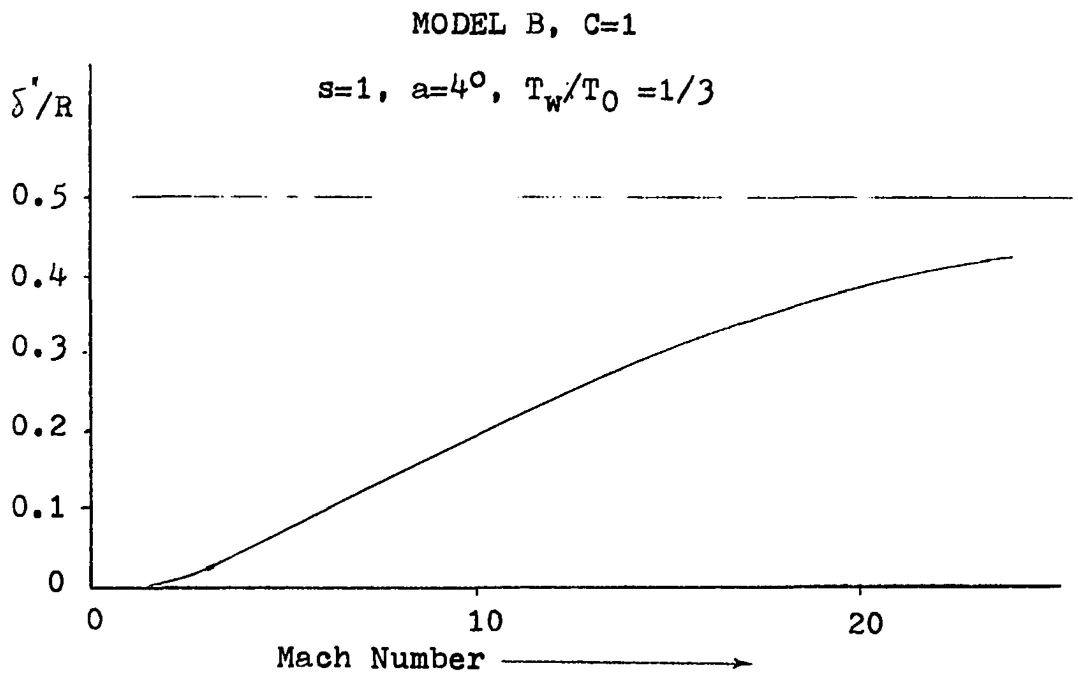

Figure 11. Model B: Displacement-Area Growth.

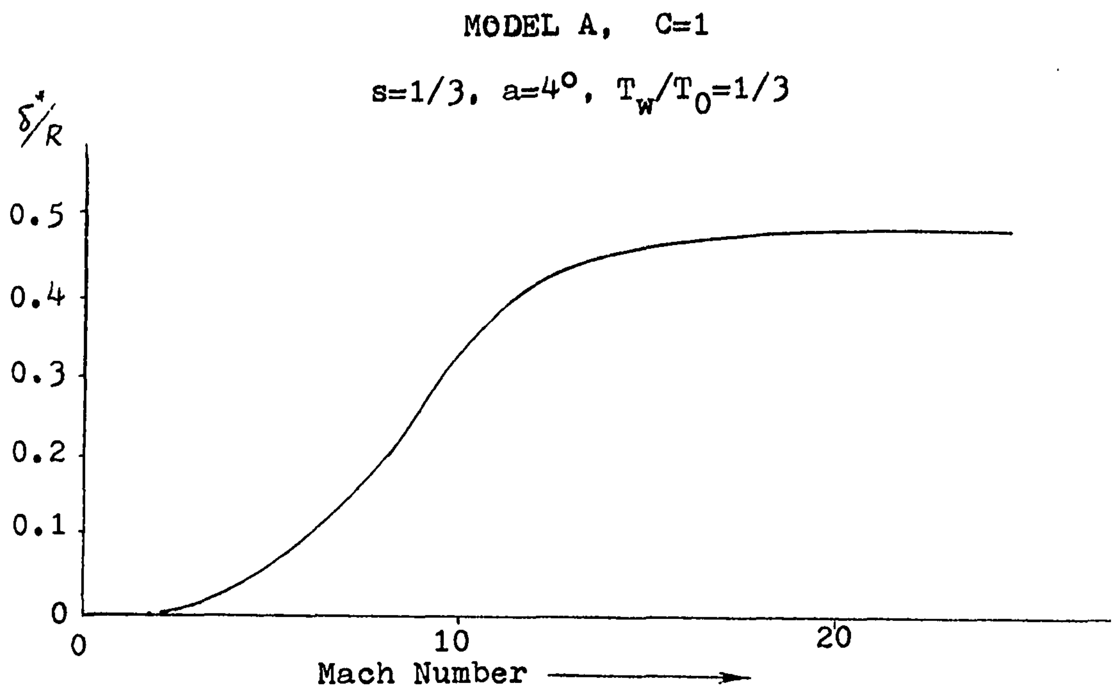

Figure 12. Model A: Displacement-Area Growth.

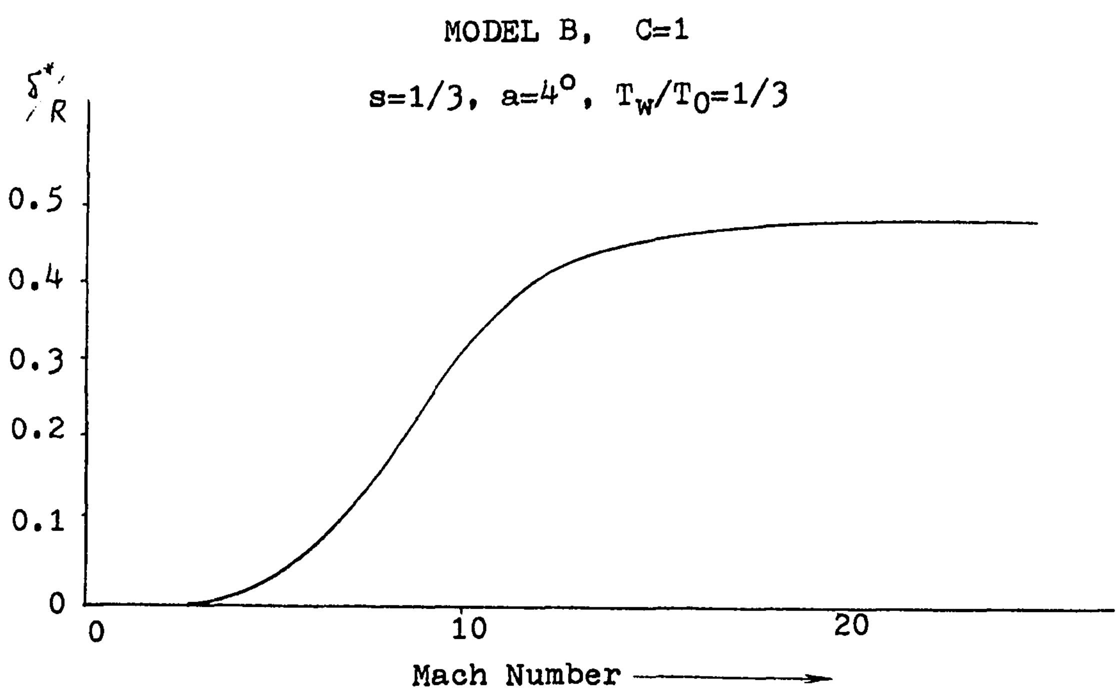

Figure 13. Model B: Displacement-Area Growth.

MODEL A, C=1

$s=1/3$, $a=4^{o}$, $T_w/T_0=1/3$

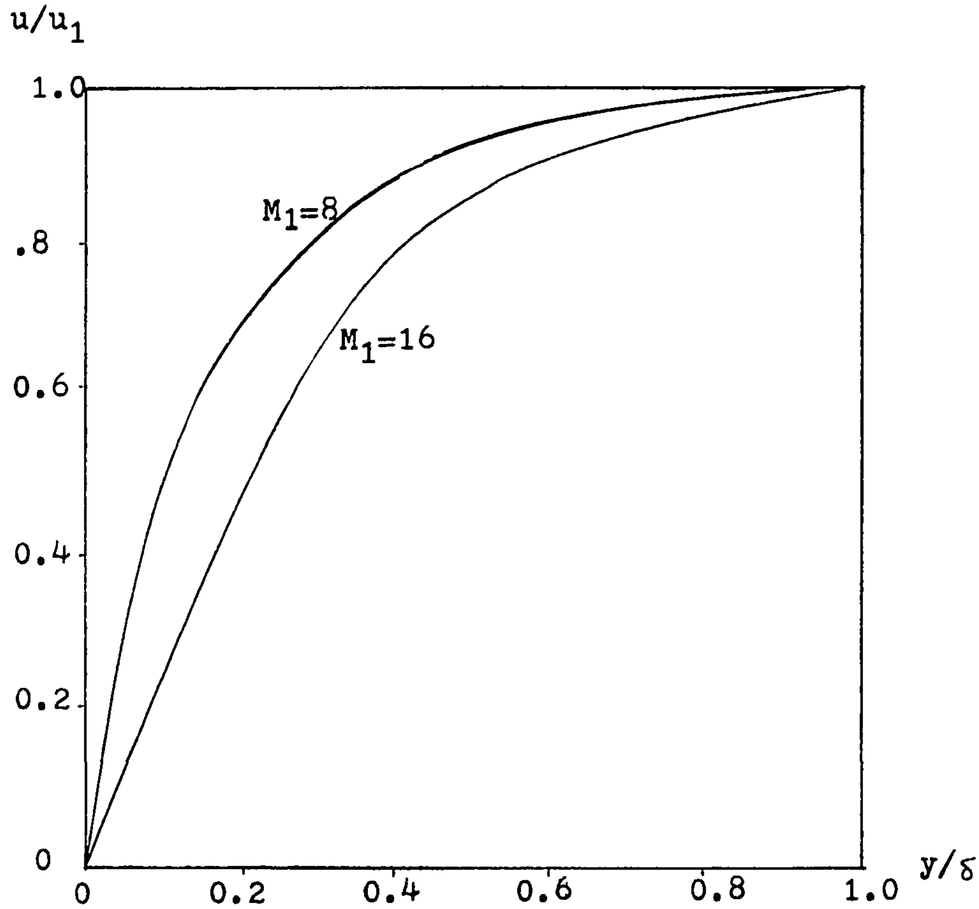

Figure 14. Model A: Velocity Profiles at M_1=8 & 16

MODEL A, C=1

$s=1/3$, $a=4^{o}$, $T_w/T_0=1/3$

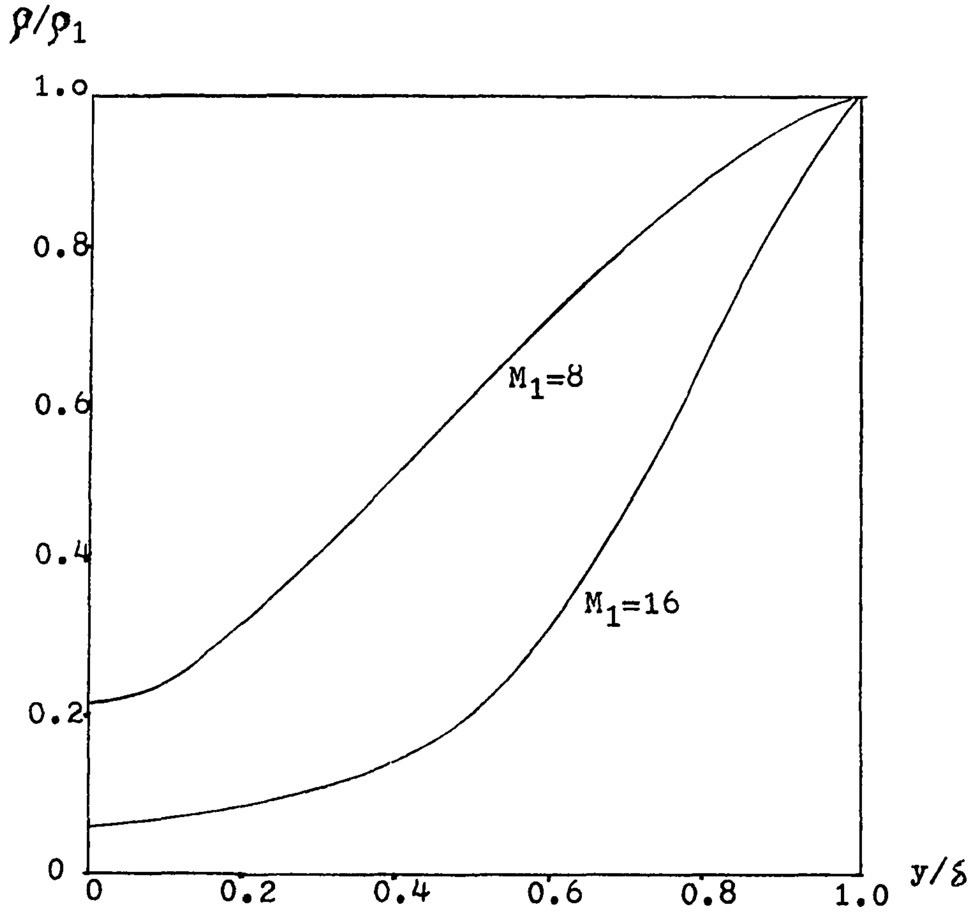

Figure 15. Model A: Density Profiles at M_1=8 & 16.

MODEL B, C=1

s=1/3, a=4°, T_w/T_0=1/3

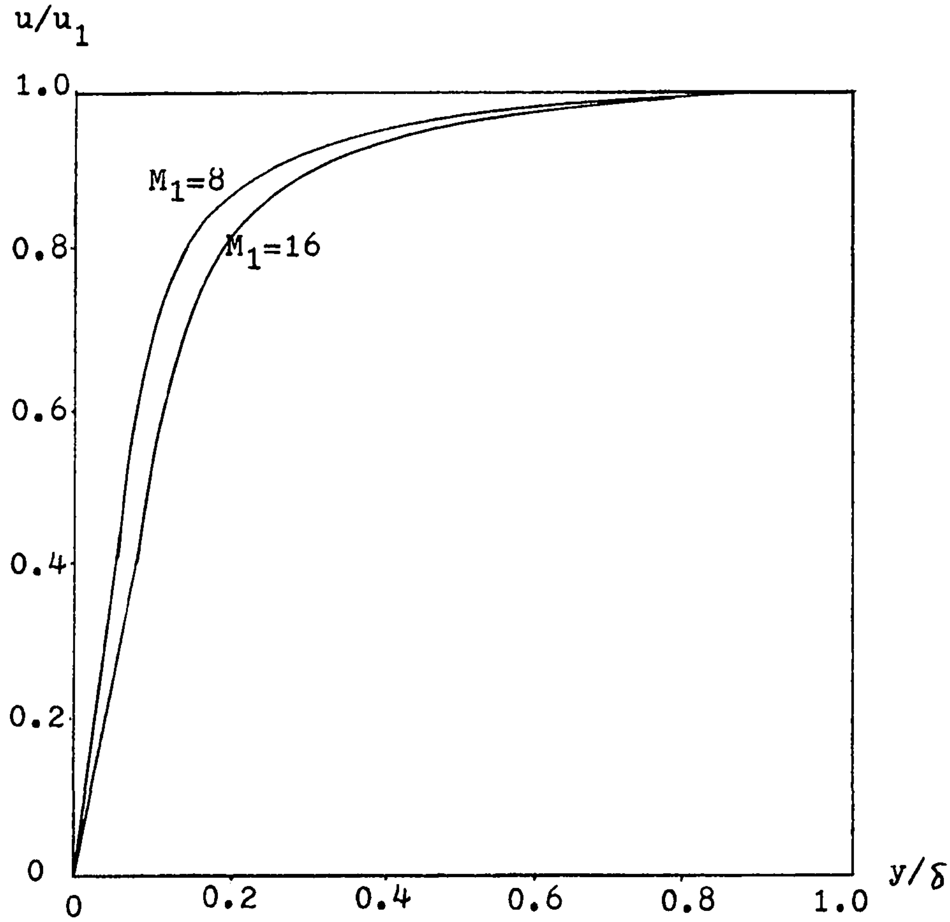

Figure 16. Model B: Velocity Profiles at M_1=8 & 16.

MODEL B, C=1

$s=1/3$, $a=4^{o}$, $T_w/T_o=1/3$

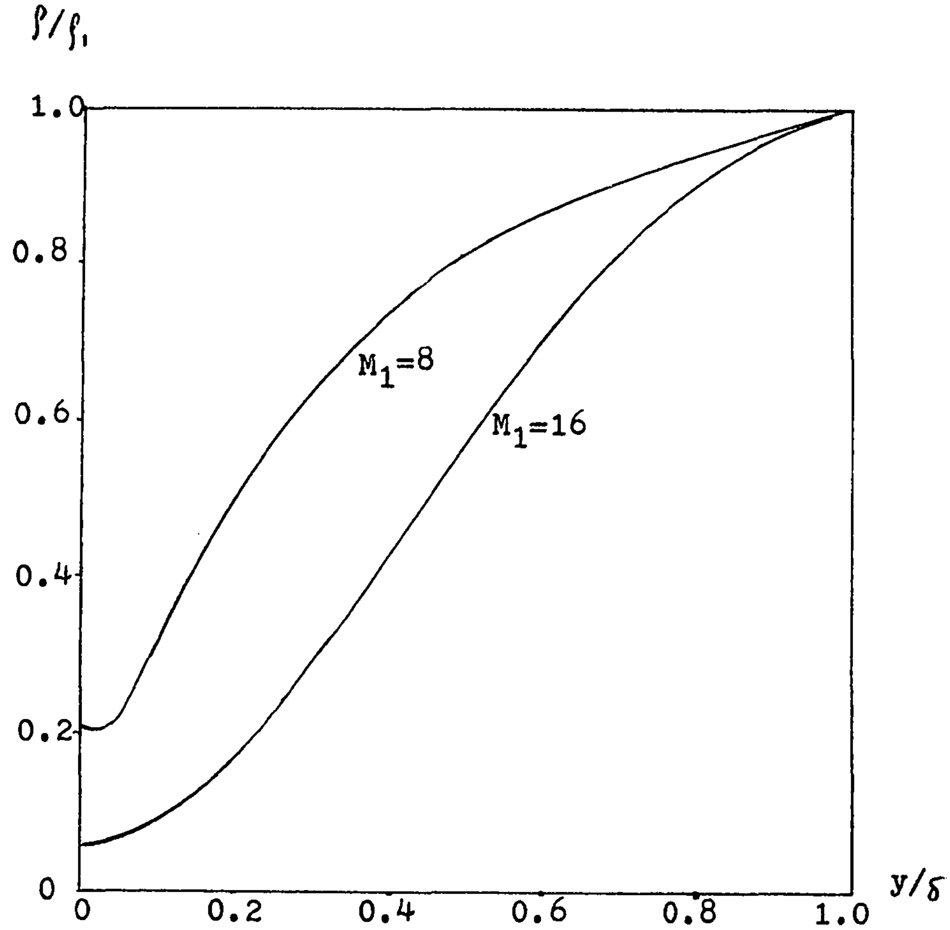

Figure 17. Model B: Density Profiles at $M_1=8$ & 16.

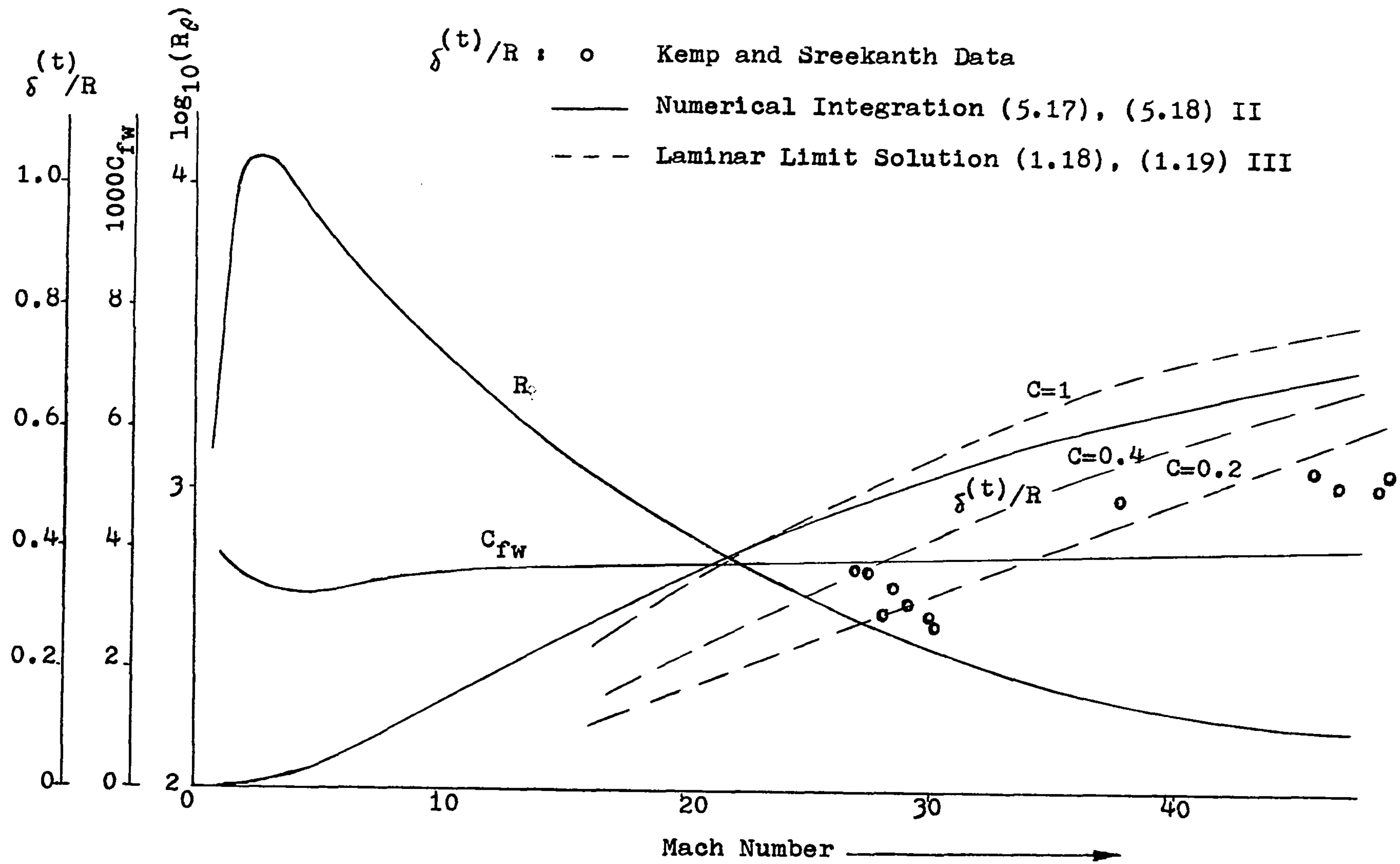

Figure 18. Linear Displacement Comparison between Asymptotic Solution Numerical Integration, and Experimental Data.

_ _ _ Kemp and Sreekanth Experimental Data

____ Numerical Integration (5.17), (5.18) II

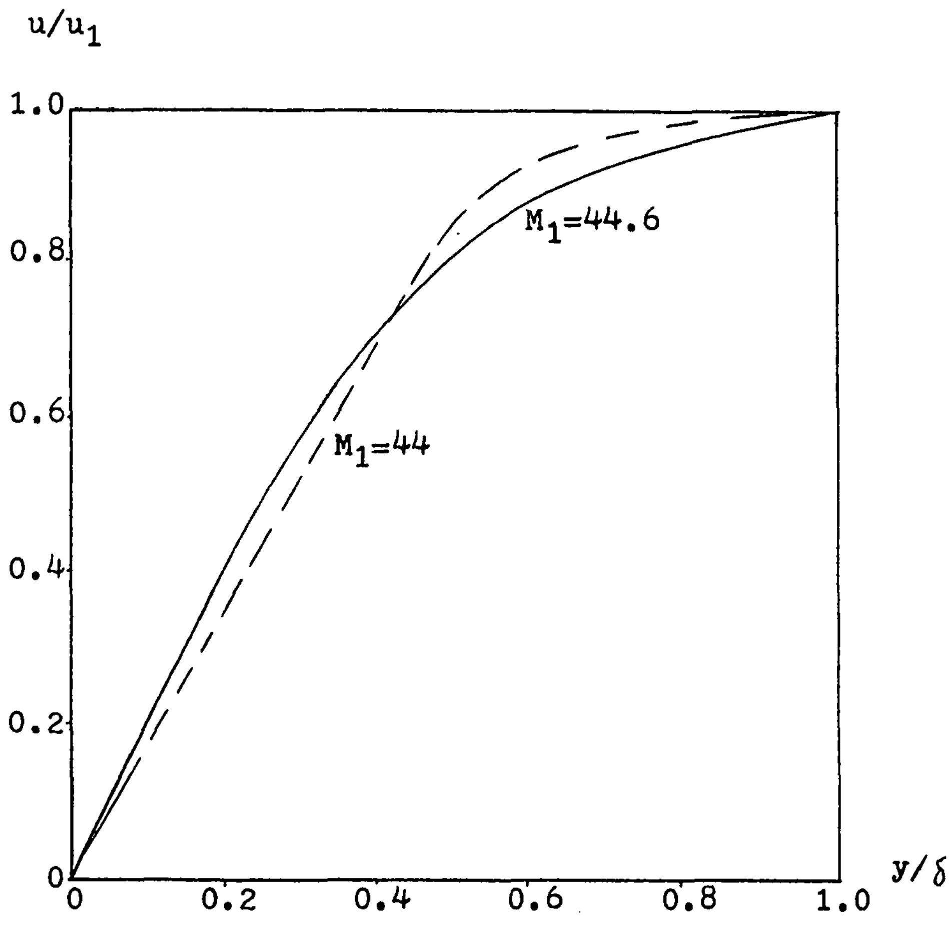

Figure 19. Comparison of Velocity Profiles.

— — — Kemp and Sreekanth Experimental Data

______ Numerical Integration (5.17), (5.18) II

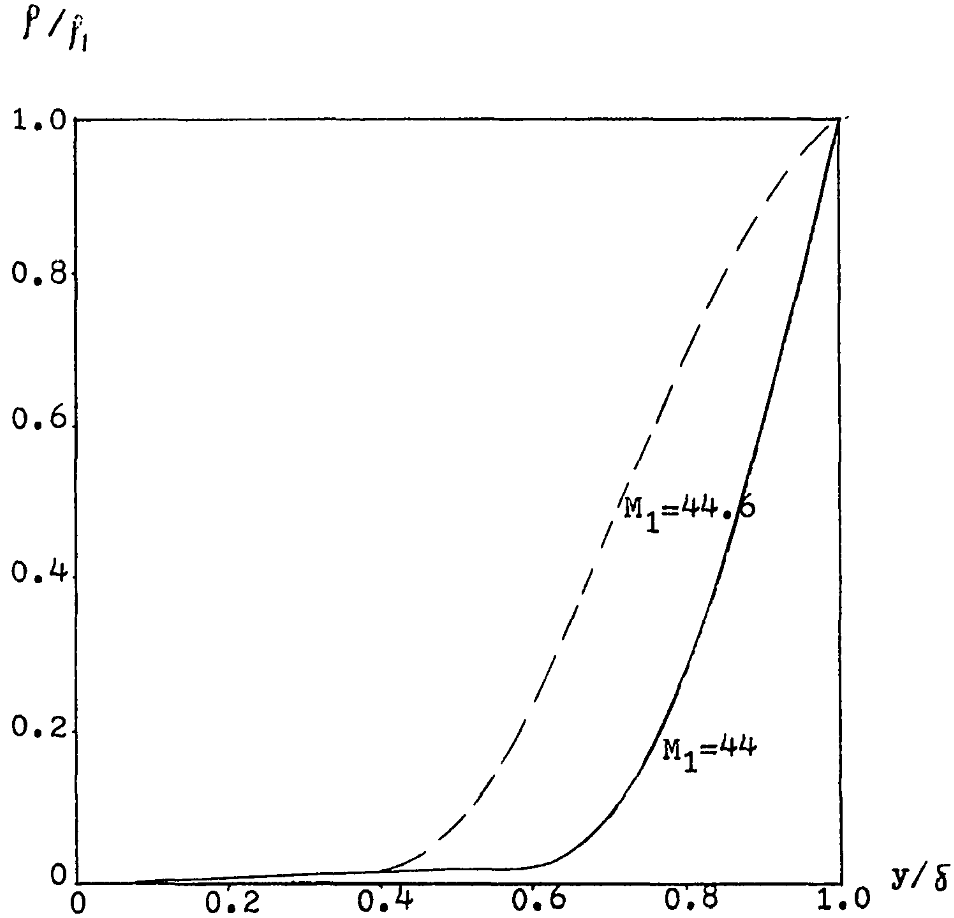

Figure 20. Comparison of Density Profiles.